Influence of junction angle on three-dimensional flow structure and bed morphology at confluent meander bends during different hydrological conditions

Riley, J. D., Rhoads, B. L., Parsons, D. R. and Johnson, K. K.

[1] Department of Geology/Geography, Eastern Illinois University, Charleston, Illinois, USA

[2] Department of Geography and Geographic Information Science, University of Illinois, Urbana, Illinois, USA

[3] Department of Geography, Environment and Earth Sciences, Faculty of Science and Engineering, University of Hull, Hull, HU67RX, UK

[4] U.S. Geological Survey, Illinois Water Science Center, Urbana, Illinois, USA

[*] Correspondence to: J. D. Riley, Department of Geology/Geography, Eastern Illinois University, Physical Science Building, 600 Lincoln Avenue, Charleston, IL 61920-3099, USA. Telephone: +1 217 581 3825. E-mail: jdriley@eiu.edu

Abstract

Recent field and modeling investigations have examined the fluvial dynamics of confluent meander bends where a straight tributary channel enters a meandering river at the apex of a bend with a 90° junction angle. Past work on confluences with asymmetrical and symmetrical planforms has shown that the angle of tributary entry has a strong influence on mutual deflection of confluent flows and the spatial extent of confluence hydro- and morphodynamic features. This paper examines three-dimensional flow structure and bed morphology for high and low momentum-flux ratios at two large, natural confluent meander bends with different tributary entry angles. At the high-junction angle confluent meander bend, mutual deflection of converging flows abruptly turns fluid from the tributary into the downstream channel, while flow in the main river is deflected away from the outer bank of the bend where a bar extends downstream of the junction corner from the inner bank of the tributary. Two counter-rotating helical cells inherited from upstream flow curvature flank the mixing interface which overlies a central pool. Substantial morphologic change due to the development of a meander cut-off upstream of the confluence during large, tributary-dominant discharge events results in displacement of the pool inward from the influx of large amounts of sediment into the confluence and substantial erosion of the point bar in the main channel. In contrast, flow deflection is less pronounced at the low-angle junction, where the converging flows almost parallel each other upon entering the confluence. A large helical cell imparted from upstream flow curvature in the main river occupies most of the downstream channel for prevailing low momentum-flux ratio conditions and a weak counter-rotating cell forms during infrequent tributary-dominant flow events. Bed

morphology remains relatively stable and does not exhibit extensive scour that often occurs at confluences with concordant beds. The mixing interface at both confluences persists through the downstream channel, indicating helical motion does not produce substantial mixing of the flows within the confluence hydrodynamic zone.

1 Introduction

The movement of water and sediment through drainage networks is invariably influenced by the merging of rivers at confluences. Flow convergence and inherent change in channel planform and geometry at junctions produce a complex hydro- and morphodynamic environment that has been the focus of substantial process-based research, including field investigations at small stream confluences (Roy et al., 1988; Roy and Bergeron, 1990; Ashmore et al., 1992; Biron et al., 1993a,b; Bristow et al., 1993; Kenworthy and Rhoads, 1995; Rhoads and Kenworthy, 1995, 1998; McLelland et al., 1996; Rhoads, 1996; DeSerres et al., 1999; Rhoads and Sukhodolov, 2001, 2004; Boyer et al., 2006; Rhoads et al., 2009) and more recently large river junctions (Best and Ashworth, 1997; Parsons et al., 2007; Szupiany et al., 2007; Lane et al., 2008; Parsons et al., 2008; Szupiany et al., 2009). Field observations, complemented by laboratory flume experiments (Mosley, 1976; Best and Reid, 1984; Best, 1986, 1987, 1988; Best and Roy, 1991; Biron et al., 1996a,b; McLelland et al., 1996), have generated empirical insights that provide the basis for testing of numerical simulations (Weerakoon and Tamai, 1989; Weerakoon et al., 1991; Bradbrook et al., 1998, 2000, 2001; Constantinescu et al., 2011) in pursuit of a comprehensive model of confluence dynamics. Collectively, this work has demonstrated the importance of confluence planform geometry (symmetrical, or **Y**-shaped, versus asymmetrical, or **y**-shaped planforms), momentum flux ratio, junction angle, and equal (concordant) or unequal (discordant) bed elevations of the confluent channels as the primary factors influencing patterns of three-dimensional (3-D) fluid motion and bed morphology at junctions.

Confluence research has focused mainly on junction planforms with straight approach channels that meet at an angular configuration before entering a straight receiving channel. However, previous field observations and studies of tributary development in meandering river systems suggest that tributaries preferentially join main channels along the outer bank of bends (Callaway, 1902; Davis, 1903; Flint, 1980; Hills, 1983; Abrahams, 1984a,b), forming confluent meander bends. Experimental work and numerical modeling of the hydrodynamics of this type of confluence planform (Roberts, 2004), complemented by recent investigation of the flow structure and bed morphology at a small natural confluent meander bend (Riley and Rhoads, 2012), have begun to reveal the effects of channel curvature on confluence dynamics.

To date, investigations of confluent meander bends have focused solely on tributaries that join a meandering river at the apex of a bend at a 90° angle (Roberts, 2004; Riley and Rhoads, 2012). Results from previous studies of the fluvial dynamics of asymmetrical and symmetrical confluences have shown that junction angle plays a critical role in controlling the degree of flow deflection and the spatial position and extent of hydrodynamic features (e.g. Mosley, 1976; Best, 1987). However, research is needed to evaluate how differences in the location and angle of tributary entry around bends influence patterns of fluid motion in confluent meander bends and to relate these patterns of fluid motion to bed morphology.

This paper examines the response of flow structure and bed morphology to hydrological events at two large confluent meander bends with different tributary entry angles in the midwestern United States. Cross-sectional measurements of 3-D velocity components were obtained for high ($M_r > 1$) and low ($M_r < 1$) momentum-flux ratio conditions to evaluate similarities and differences in fluid motion and bed morphology at high- and low-angle junctions. This study is also the first to document tributary-dominant flow conditions (M_r > 1) at natural confluent meander bends, which have been shown to significantly rearrange bed morphology at other confluences (Best, 1988; Biron et al., 1993b; Rhoads and Kenworthy, 1995, 1998; Rhoads, 1996; Rhoads et al., 2009). The results provide critical information on the response of flow and morphologic features to variation in geometric and hydrological controlling factors, and contribute to the advancement of a comprehensive model of confluent meander bend dynamics.

2 Field sites

Two confluent meander bends with different junction angles along the Wabash River were selected as study sites for the research (Figure 1). At its mouth, the Wabash River (WR) joins the Ohio River (OR) slightly upstream of the apex of a meander bend at a junction angle of approximately 90°. At the confluence, the drainage area of the Ohio River (279,719 km^2) is over three times greater than the drainage area of the Wabash River (85,237 km^2). Differences in drainage area and the geographic extent of the watersheds result in disparities in the magnitude and timing of peak flows between the rivers at the junction. Wabash Island lies directly across from the mouth of the Wabash River and divides flow in the Ohio River into two channels upstream of the confluence. The main channel into which the Wabash River enters transports about two-thirds of the flow around the north side of the island, which comprises the inner bank of the meander bend. The width of this channel varies from 500 m in the curving upstream channel to about 675 m downstream of the confluence. The Wabash River bends sharply as it joins the Ohio River. Channel width increases from 300 m upstream of the junction to 475 m at the mouth of the river. Maximum channel depth at the mouth of the Wabash River is approximately 10.5 m, whereas maximum depths in the Ohio River are as great as 15 m.

The John T. Myers Locks and Dam is 3.2 km upstream of the junction on the Ohio River, but does not disrupt patterns of flow at the confluence. The United States Army Corps of Engineers (USACE) periodically dredges the navigation channel to maintain adequate depth for barge traffic, but the bed morphology is highly responsive to sediment fluxes into the confluence (Zinger et al., 2011). Downstream of a mainstream reservoir in its headwaters, the Wabash River flows unimpeded for 661 km to the Ohio River. The average channel gradient of the Wabash River upstream of the confluence (0.0003) is steeper than the gradient of the Ohio River (0.0001) below the John T. Myers Locks and Dam. Bed material at the site is comprised primarily of coarse sand with fine gravel.

The second study site provides a contrast in tributary entry angle compared to the high-angle confluent meander bend of the Ohio and Wabash Rivers (ORWR). The confluence of the Wabash River and Vermilion River (WRVR) is located 375 km upstream of ORWR in west central Indiana. At this location, the drainage area of the Wabash River (21,481 km^2) is nearly six times larger than the drainage area of the Vermilion River (3,714 km^2). The Vermilion River enters the Wabash River downstream of the apex of a meander bend on the Wabash River at an angle of 36°. The tributary is relatively straight and aligned with the downstream channel, whereas the main channel curves sharply immediately upstream of the confluence. The Vermilion River is about 60 m wide at its mouth, whereas the Wabash River is approximately 140 m wide. Bankfull channel depth is about 6 m in the Vermilion River and 6-8 m in the Wabash River. Average channel gradients upstream of the confluence are 0.00007 for the Wabash River and 0.0001 for the Vermilion River. Bed material at the junction consists of a mixture of coarse sand and gravel.

3 Field methods and data analysis

Field data for the two study sites included measurements of incoming flow, 3-D velocities, near-surface temperatures, and bed morphology. Measurements of discharge and mean velocity obtained at two cross sections of the confluent rivers immediately upstream of each junction were used to compute the momentum-flux ratio (M_r) of the incoming flows:

$$M_r = \frac{\rho Q_2 U_2}{\rho Q_1 U_1} \quad (1)$$

where ρ is flow density (kg m^{-3}), Q is discharge (m^3 s^{-1}), U is mean cross-sectional velocity (m s^{-1}), and the subscripts 1 and 2 refer to the main river and tributary, respectively. Water-surface elevations during periods of field measurements at ORWR were determined from stage data for the JT Myers L/D lower gage on the Ohio River. At WRVR, water-surface elevations were surveyed on the Wabash River near the upstream junction corner at the beginning and end of each measurement campaign.

Three-dimensional velocity, water temperature, and bathymetry data were obtained at several cross sections distributed throughout each confluence. Cross sections were located upstream of the confluence on the tributary and main channels to characterize inherited flow structure, within the central region of the junction, and across the downstream channel (Figure 1). Cross sections were generally positioned 40-50 m apart through the center of WRVR and 75-100 m apart upstream and downstream of the junction. Central cross sections at ORWR were 50-150 m apart, whereas the distance between cross sections on the upstream and downstream channels varied from 150 to 500 m. Cross sections at both sites were oriented orthogonally to the direction of the local centerline of either the main channel or the tributary.

Simultaneous measurements of downstream, cross-stream, and vertical velocities and bottom depth were obtained at each cross section with an acoustic Doppler current profiler (ADCP). A Workhorse Rio Grande ADCP manufactured by Teledyne RD Instruments (TDRI) was used to collect data along channel cross sections via a moving-boat deployment, similar to methods used in previous studies of coherent flow structures in rivers (Richardson and Thorne 1998; McLelland et al., 1999; Muste et al., 2004; Dinehart and Burau, 2005a,b; Parsons et al., 2005; Parsons et al., 2007; Szupiany et al., 2007). The ADCP was attached to a mount on the port side of the bow of a 5.79 m long, aluminum-hull boat. The four transducers of the ADCP were positioned 0.15-0.27 m below the water surface depending on flow conditions during each survey date. The ADCP cannot measure velocities within a transmit blanking distance of about 0.5 m below the transducers. Also, the bottom ~6% of the measured flow depth was removed due to acoustic side-lobe interference in the near bed returns. The sampling interval of the ADCP ranged between 1.3-1.7 s and vertical bin sizes were either 0.1 m or 0.25 m within each ping ensemble. A 1200 kHz ADCP was used for measurement during low-momentum flux ratio flows ($M_r < 1$), whereas a 600 kHz ADCP was used to survey high-momentum flux ratio conditions ($M_r > 1$) to prevent signal loss associated with high acoustic backscatter caused by high levels of suspended sediment concentrations.

Boat position and velocity were determined using a differential global positioning system (DGPS) receiver. The DGPS-receiver provides time-stamped geographic coordinates at 10 Hz with up to sub-meter accuracy and was integrated with the ADCP to fully georeference velocity data at each ensemble. Real-time GPS data were also used to navigate the boat as accurately as possible along the predetermined cross sections, using Hypack™. The DGPS-antenna was affixed to the port side mount directly above the ADCP.

Following recommendations from Szupiany et al. (2007), multiple traverses, or transects, of each cross section were surveyed to obtain spatially and temporally averaged values of velocity and to resolve details of secondary-flow patterns, while minimizing disturbances arising from turbulent velocity fluctuations and boat motion. At WRVR, measurements were typically repeated for five transects at each cross section in the field. Wide channel cross sections at ORWR increased the total time needed to survey each cross section. Thus, repeat measurements were limited to either two or four transects per cross section.

The Velocity Mapping Toolbox (VMT), an ADCP post-processing software package, was used to compute spatially and temporally averaged velocity data for each cross section from repeat transect measurements (Parsons et al., 2013). Velocity ensembles were interpolated to grid nodes using a least-squares regression line fit through transects at each cross section. Time-averaged values of downstream (U), cross-stream (V), and vertical (W) velocity were computed for bins within each ensemble in relation to the cross-section orientation. These velocity components were used to derive depth-averaged vector plots of downstream and cross-stream velocities for the junctions on each measurement date and contour plots of downstream velocity superimposed with cross-stream/vertical velocity vectors for individual cross sections. To identify secondary flow structures within complex converging flows at confluences, VMT also rotates velocity vectors for each bin in an ensemble to the direction of the depth-averaged velocity vector for that ensemble. Secondary flow is then defined by velocity components perpendicular to this rotation. Previous studies of confluence hydrodynamics have used this rotation method (Rozovskii, 1957) to detect helical motion in strongly converging flows (Rhoads and Kenworthy, 1998; Lane et al., 2000).

Measurements of near-surface water temperature were recorded at each ensemble by the ADCP transducer head. Deviations between water temperatures at each ensemble and the mean temperature for the respective cross section were computed to limit the effect of diurnal variation in water temperature during the surveys. The normalized data were spatially interpolated by kriging to produce contour plots of near-surface temperature patterns on each measurement date. The mixing interface is defined by the location where temperature deviation from the cross-sectional mean is zero.

Reflections of acoustic beams emitted by the ADCP transducers from the channel bottom were used to produce cross-section plots of bed morphology and bathymetric maps of each confluence. Bed profiles for each averaged cross section were developed by computing in VMT a weighted average of the 4-beam depths at each ensemble and converting depths to elevations based on flow stage data. Besides data from the cross section surveys, longitudinal transects throughout each confluence yielded additional bathymetric data for mapping the topography of the channel bed. Topographic maps of the bed morphology at the junctions were generated by kriging and contouring bed elevation data collected at all transects on each survey date.

4 Results

4.1 Hydrologic and hydraulic conditions

Field data on 3-D velocity fields and bed morphology were collected on two dates during different hydrological conditions at both sites: May 15, 2008 and January 6, 2009 at ORWR and January 9, 2007 and February 6, 2008 at WRVR. Hydrologic variability prior to and during the field campaign was estimated by deriving the normalized flood dominance ratio (Zinger et al., 2013), a modified discharge ratio of the converging flows scaled by a formative discharge event for the tributary channel from mean daily discharge data recorded at upstream river gages. The normalized flood dominance ratio is calculated as:

$$F_d = \left(\frac{Q_2}{Q_1} / Q_{2\ \mathrm{bankfull}}\right) \times Q_2 \quad (2)$$

where Q is discharge ($m^3\ s^{-1}$) and the subscripts 1 and 2 refer to the main river (Ohio River at ORWR, Wabash River at WRVR) and tributary (Wabash River at ORWR, Vermilion River at WRVR), respectively. Plots of F_d against time provide a hydrological context for the ADCP measurement campaigns, and duration curves of index values derived for the periods of record from the upstream river gages show the frequency of the events measured in this study (Figure 2).

At ORWR, low momentum-flux ratio conditions (M_r < 1) prevailed on May 15, 2008 (Table 1) during the rising stages of a hydrologic event produced by heavy precipitation throughout the Midwest in early May. Flow stage increased by 0.12 m at the JT Myers L/D lower gage during 7.5 hours of data collection. A series of tributary-dominant discharge events (Q_r > 1) followed during the late spring and summer of 2008 (Figure 3A). A second set of velocity data was collected on January 6, 2009 during high momentum-flux ratio conditions resulting from snowmelt and intense rainfall generated by severe thunderstorms across the central and southern portions of the Wabash River drainage basin during late December 2008. Measurements were obtained over a 5-hour period during which stage decreased by 0.11 m.

Tributary-dominant flow conditions are infrequent and short-lived at WRVR (Figures 3B,D). A period of sustained low discharge ratio conditions preceded the survey on January 9, 2007 (Figure 3B). Changes in stage were minor during measurement, dropping just 0.02 m over 5.5 hours. In contrast, surface runoff from thunderstorms over a widespread snowpack resulted in flooding throughout much of the Vermilion River drainage basin and produced flows with M_r > 1 at the confluence on February 6, 2008 (Table 2). Data were collected over 6 hours during the rising stages of this event, in which water levels increased by 0.5 m.

4.2 Bed morphology

General morphological features and adjustment of the bed to varying flow conditions differ between the field sites. At ORWR, patterns of bed morphology on May 15, 2008 include the pool of the Ohio River's navigation channel within the central region of the junction flanked by a broad point bar along the inner (south) portion of the bend and a long bar platform on the north side of the channel protruding slightly into the confluence from the Wabash River and extending below the downstream junction corner (Figure 3A). The pool turns inward at the upstream junction corner from a position against the outer bank, resulting in progressive symmetry of channel cross-section profiles through the center of the confluence and upstream end of the downstream channel (Figure 4, cross-sections L, N, and O). The pool shifts back toward the outer bank farther downstream (Figure 3A, cross-section Q). In the curving tributary channel, a bar wraps around the inner (west) bank of the bend and a pool is located along the outer (east) bank, leading to channel asymmetry (Figure 4, cross-sections A-C).

Large tributary-dominant discharge events and widespread flooding during June 2008 produced a meander cutoff approximately 2 km upstream of the junction on the Wabash River (Zinger et al., 2011). Large amounts of eroded sediment were transported downstream from the cutoff into the confluence and significantly altered the bed morphology. The United States Army Corps of Engineers surveyed the bed topography of the Ohio River with an echo sounder on June 23, 2008, before dredging the deposited material from the navigation channel.

The survey data for June 23, 2008 show that a wedge of sediment extends from the mouth of the tributary across the outer (north) half of the main channel and into the central region of the junction (Figure 3B, cross-sections K-N). The influx of sediment increased local bed elevations by over 6 m compared to May 15, 2008 and bisected the pool. The upstream segment of the pool is confined to a narrow zone between the upstream edge of the sediment wedge and the inner bank point bar. Scouring of the point bar has occurred across the channel from the tributary entrance (Figure 3B, cross-sections K and L), but this scouring along the inner bank does not extend into the downstream channel (cross-sections M-P). The downstream portion of the pool within the bend is still located near the outer bank (cross-sections O-Q).

The bathymetric data for January 6, 2009 show that the influx of sediment from the Wabash River persisted, producing a bed topography similar to that in June 2008. For the most part, the pool has the same alignment through the junction on the two dates, but the thalweg is wider and shifted closer to the outer bank in January 2009 than in June 2008 (Figures 3B,C). As a result, the point bar is truncated by the pool toward the inner bank of the bend. Across the channel, the distinctiveness of the sediment wedge has diminished; instead an elongated body of sediment wraps around the downstream junction corner and extends downstream along the outer bank of the bend in the Ohio River (Figures 3B,C). Patterns of bed morphology in the tributary channel remain comparatively unchanged, although aggradation is evident along the inner bank at cross-section A (Figure 4).

In contrast, morphological features at WRVR are similar on both measurement dates (Figure 5). A wide pool spans the center and outer (west) portion of the main channel upstream of the confluence. This pool ends within the confluence as the bed rises gradually by about 1.5 m from the deepest part of the thalweg upstream. A prominent point bar exists along the inner bank of the bend and a small region of scour is evident immediately downstream from the upstream junction corner (Figure 5). At the apex of the bend, the point bar narrows where the pool width is greatest, but widens through the confluence and the downstream channel. Minor degradation of the bar occurred between the January 9, 2007 and February 6, 2008 surveys (Figure 6, cross-sections J, K, and M) with up to 1 m of material excavated from the bar face in the confluence (cross-section J). The downstream end of the pool is shifted toward the center of the main channel and tapers where the tributary enters the confluence (Figure 5, cross-sections J and K). A low ridge on the bed separates the shallow scour hole in the confluence from the thalweg of the Wabash River (Figure 7, cross-section K). This ridge gradually widens into a broad platform extending across much of the channel downstream (cross-section M). Scour along the outer bank and in the center of the channel occurs downstream of the platform (cross-section N).

4.3 Depth-averaged velocity

The degree of convergence between depth-averaged velocity vectors and corresponding flow deflection along the mixing interface differ significantly between the field sites. At ORWR, curvature both of the main channel and tributary immediately upstream of the junction, along with the curved planform of the downstream channel, produces complex spatial patterns of velocity vectors (Figure 7). The high-angle entrance of the Wabash River into the Ohio River initiates strong flow deflection through the central region of the confluence. On both measurement dates, the mixing interface is defined approximately by the boundary between inward oriented vectors reflecting penetration of flow from the Wabash River into the confluence and vectors that align with the curved planform of the Ohio River through the center of the channel and along the inner (south) bank (cross-sections J-N). Flow from the Wabash River is turned rapidly to align with the Ohio River immediately downstream of the confluence (cross-section O) and deflects vectors in the Ohio River away from the outer (north) bank of the meander bend. Vector magnitudes progressively increase through the confluence as the flows combine and accelerate, and are greatest through the center of the downstream channel (cross-sections O and P).

Low momentum-flux ratio conditions on May 15, 2008 (M_r < 1) result in a distinct mixing interface on the tributary side of the channel characterized by abrupt lateral change in vector magnitudes, rapid change in orientation of velocity vectors characterizing flow from the tributary into the confluence, and minimal outward deflection of vectors in the main river (Figure 7A, cross-section L). Flow from the Wabash River is narrowly confined between the mixing interface and the outer (north) bank of the meander bend upon entering the confluence (cross-sections L and N), whereas high velocity flow in the Ohio River occupies most of the channel. A region of low velocities along the outer (east) bank of the curving Wabash River (cross-sections B-D) defines an elongated zone of flow stagnation extending upstream from the junction. The stagnation zone displaces the largest flow vectors in the Wabash River from the outer bank (cross-section A) to the inner (west) bank (cross-section D) as flow from this tributary enters the Ohio River. Flow accelerates across nearly the entire channel cross section at the downstream end of the junction (cross-section N). Farther downstream (cross-sections O-Q), the largest velocities are positioned between the center of the channel and a small zone of low-velocity flow that develops against the outer bank.

During high momentum-flux ratio conditions on January 6, 2009 (M_r > 1), strong penetration of flow from the Wabash River into the confluence shifts the mixing interface toward the inner (south) bank (Figure 7B) compared to conditions for $M_r < 1$. Low velocity flow entering the junction from the Ohio River (cross-section J) is restricted to the inner part of the channel, where it accelerates to maintain continuity (cross-sections K and L). A large mid-channel bar that developed in the Wabash River between the survey dates in response to a meander cutoff immediately upstream (Zinger et al., 2011) produces strong flow convergence downstream of this feature (cross-section A). Large depth-averaged velocities persist over the central and outer (east) portion of the tributary channel (cross-section B), but flow in this part of the channel decelerates immediately upstream of the confluence (cross-sections C and E). Spatial patterns of tributary vectors near the mouth are aligned obliquely to the orientation of cross-sections K-M, indicating pronounced penetration of tributary flow into the confluence. The flow stagnation zone observed on May 15, 2008 is absent from the tributary channel. Instead, deceleration of flow occurs over the outer (north) portion of the Ohio River near the junction apex (cross-section J). Downstream of the confluence, a region of separated flow exists along the outer bank and the largest velocity vectors span the center and inner half of the channel (cross-sections O and P).

In contrast to vector patterns at ORWR, the low-angle entrance of the Vermilion River at WRVR leads to patterns of depth-averaged velocity vectors between the main river and tributary that are almost parallel to each other upon entering the confluence (Figure 8). Consequently, mutual deflection of the converging flows is much less pronounced than at ORWR. The mixing interface is readily discerned from abrupt differences in vector magnitudes between the rivers on both measurement dates (cross-sections J-M). Flow curvature in the Wabash River upstream of the confluence is defined by a transverse gradient in depth-averaged velocities in which the largest vectors occur over the east side of the bend upstream of, at, and slightly downstream of the bend apex (cross-sections F-I). Depth-averaged velocities increase through the confluence and quickly align with the orientation of the downstream channel. The low junction angle of the confluence restricts flow from the Vermilion River to the outer (west) portion of the downstream channel. Flow separation from the outer bank of the downstream channel was not observed on either date.

Dominant flow from the Wabash River occupies most of the confluence when $M_r < 1$ on January 9, 2007 (Figure 8A). The mixing interface shifts rapidly outward through the junction, coinciding with the transition of maximum depth-averaged velocities in the Wabash River from the inner (east) bank to the center of the downstream channel (cross-sections J-M). Low velocity flow occurs across the entire tributary (cross-sections A and B) and is confined against the outer (west) bank of the receiving channel. A narrow zone of small vectors associated with this tributary flow diminishes abruptly downstream of the confluence (cross-sections L and M).

Increased penetration of flow from the Vermilion River into the downstream channel forces the mixing interface toward the inner bank of the bend when $M_r > 1$ on February 8, 2008 (Figure 8B). High-velocity flow from the tributary prevents flow from the Wabash River from expanding outward across most of the flow width as on the previous measurement date. Instead, flow accelerates over the outer portion of the channel and an abrupt transition in vector magnitudes along the mixing interface persists well downstream of the confluence (cross-sections J-N). Deceleration of flow along the outer bank of the Wabash River upstream of the confluence is pronounced on this date, resulting in flow stagnation near the upstream junction corner (cross-section I).

4.4 Downstream and cross-stream velocity

Spatial patterns of downstream and cross-stream velocity vectors at ORWR are responsive to shifts in momentum flux ratio. Upstream of the junction, the downstream velocity field (U) is characterized by high-velocity cores in the Ohio and Wabash Rivers that are separated by a region of low-velocity fluid surrounding the junction apex. Flow stagnation extends upstream along the outer (east) bank of the Wabash River when M_r < 1 (May 15, 2008) (Figure 9A, cross-section D). This region of stagnation generates a cross-stream pressure gradient that shifts the high-velocity core of the tributary from a position near the outer bank of the bend (cross-section A) to the inner (west) portion of the channel (cross-section D) as flow enters the Ohio River. Velocities are also small near the junction apex in the Ohio River, where the zone of stagnation is narrowly confined against the outer (north) bank (cross-section I). When M_r > 1 (January 6, 2009), increased penetration of tributary flow into the confluence shifts most of the stagnation zone around the junction apex to the outer portion of the channel cross-section of the Ohio River, confining the highest downstream velocities in the main channel to the inside of the meander bend (cross-section J).

The channels of both rivers bend immediately upstream of the junction, resulting in curvature-induced secondary circulation within the converging flows on both measurement dates. Secondary velocity vectors (V_s), derived using the Rozovskii method, reveal the presence of a helical cell with clockwise circulation (looking upstream) in the Wabash River spanning most of the channel cross-section on May 15, 2008 (Figure 9A, cross-section A and D). A small counter-rotating cell is apparent next to the outer (east) bank upstream of the stagnation zone (cross-section A). On January 6, 2009, the development of a mid-channel bar in the tributary following cutoff of the bend upstream of the junction confines the main helical cell between the bar face at the center of the channel and the outer bank (Figure 9B, cross-section A). The resulting decrease in channel area accelerates the flow and intensifies helical motion in the thalweg. Channel width increases at the mouth of the tributary and patterns of secondary circulation become less coherent (Figure 9B, cross-section E). Large-scale secondary circulation is also present in the Ohio River upon entering the confluence, where a counterclockwise rotating helical cell extends across most of the incoming flow on both measurement dates (Figure 9A, cross-section I; Figure 9B, cross-section J).

Helicity from curving flow upstream in each river persists through the center of the confluence and is characterized by side-by-side counter-rotating, surface-convergent helical cells (Figures 9A,B, cross-sections L-O). The cell on the south side of the confluence that originates in the Ohio River shifts away from the mouth of the tributary, especially when $M_r > 1$ (Figures 9A,B, cross-sections L and N). The helical cell originating in the Wabash River is confined to the north side of the confluence as flow from this tributary is forced to turn rapidly into the downstream channel. The spatial extent of this cell is smaller for $M_r < 1$ (Figure 9A, cross-sections L and N) than for $M_r > 1$, when flow from the Wabash River penetrates far into the confluence (Figure 9B, cross-section L and N). On both measurement dates, mutual deflection of flow between the tributary and main channel reinforces the upstream patterns of flow curvature, thereby strengthening fluid rotation within the counter-rotating helical cells within the confluence. Consequently, the transfer of downstream momentum is enhanced laterally toward the mixing interface, which is generally positioned between the twin helical cells and identified by a distinct difference in near-surface water temperatures of the two rivers (Figure 10).

The combined flows accelerate through the downstream channel on both measurement dates, but differences in the spatial extent of the helical cells and the size of a zone of flow separation at the downstream junction corner are seemingly controlled by momentum flux ratio. The well-organized counterclockwise-rotating helical cell inherited from upstream flow curvature in the Ohio River extends across nearly three-quarters of the flow width in the downstream channel when $M_r < 1$ (Figure 9A, cross-sections O and P). Lateral advection of downstream momentum by this helical cell directs near-surface high velocity fluid across the channel toward the mixing interface, which is positioned near the outer margin of the high downstream velocity core. Along the flanks of the mixing interface, fluid plunges toward the bed. Confinement of the mixing interface near the outer (north) bank (Figure 10A) restricts the smaller helical cell within flow from the Wabash River to the outer portion of the bend. The clockwise circulation of this helical cell weakens and the cell decreases in size farther downstream (cross-section P). A small zone of low downstream velocities representing flow separation from the downstream junction corner develops adjacent to this cell along the outer bank (cross-sections O and P).

When $M_r > 1$, increased penetration of tributary flow into the confluence and subsequent shifting of the mixing interface to the center of the channel (Figure 10B) enhances flow separation along the outer (north) bank downstream from the tributary entrance (Figure 9B, cross-sections O and P). The helical cell on the tributary side of the channel extends inward from the separation zone across more than half of the downstream channel (cross-section P). The opposing helical cell is confined to the inner (south) portion of the channel and is clearly smaller than for $M_r < 1$. The counter-rotating cells are similar in size at the entrance of the downstream channel (cross-section N) and transfer downstream momentum laterally to the center of the channel cross-section where the combined flows accelerate. Further downstream (cross-section P), patterns of secondary circulation become less organized as the hydraulic effects of the confluence on the flow begin to wane.

The comparatively low junction angle at WRVR results in less direct flow deflection between the converging rivers and less complex patterns of downstream and cross-stream velocity vectors than at ORWR. The curving channel planform of the Wabash River upstream of the confluence subjects flow to an outward-directed centrifugal force. Near-surface secondary velocity vectors are oriented outward, and a counterbalancing pressure gradient force directs near-bed vectors inward, initiating counterclockwise helical motion of the flow across most of the main channel on both measurement dates (Figures 11A,B, cross-sections F and I). For $M_r < 1$ (January 9, 2007), a core of high downstream velocity in the Wabash River upstream of the confluence expands from the center and inner (east) portion of the channel (Figure 11A, cross-section F) toward the outer (west) bank at the entrance to the confluence (cross-section I), whereas low velocities extend across the entire mouth of the Vermilion River (cross-section B). For $M_r > 1$ (February 6, 2008), the highest downstream velocities in the Wabash River upstream of the confluence are located toward the inside of the meander bend due to the development of a zone of flow stagnation that extends upstream from the junction apex along the outer bank of the bend (Figure 11B, cross-sections F and I). Downstream velocities exceed 1.5 m s^{-1} across most of the flow width of the tributary (cross-section B).

Contrasts in both downstream velocity and surficial water temperature between the converging flows define the position of the mixing interface through the central region of the confluence on both measurement dates (Figures 11A, 12A, cross-section J; Figures 11B, 12B, cross-sections J and K). Low velocity flow from the tributary is confined against the outer (west) bank by the outward expansion of the core of high velocity from the Wabash River when $M_r < 1$ (Figure 11A, cross-sections J-K). Downstream, the velocity differential between the flows diminishes (cross-sections K-N), even though the contrast in surficial water temperature lingers (Figure 12A), suggesting the mixing interface remains well-defined and precludes mixing of the contiguous flows in the vicinity of the junction. Temperature data show that the path of the mixing interface, although somewhat irregular, generally bows outward following a curved path that represents a continuation of the curving outer bank of the Wabash River upstream of the confluence.

The channel of the Vermilion River is relatively straight and aligns with the downstream channel of the Wabash River such that curvature of tributary flow at the confluence is minimal. The pattern of secondary flow within the tributary is disorganized and does not provide clear evidence of large-scale secondary motion when $M_r < 1$ (Figure 11A, cross-section B). Instead, a counterclockwise-rotating helical cell inherited from curving flow upstream in the Wabash River occupies all but the outermost portion of the channel cross section upon entering the confluence (cross-section J). This large helical cell advects high-momentum fluid laterally to the tributary side of the mixing interface and is well organized in the downstream channel (cross-sections M and N) despite a lack of mixing near the surface (Figure 12A).

Flow deflection by the Vermilion River is enhanced when M_r >1 and shifts the mixing interface more than 25 m toward the inner (east) bank in the downstream channel compared to its location when M_r < 1 (Figure 12B, cross-sections M and N). The mixing interface aligns with the inner margin of the high-velocity core from the tributary, which persists through the confluence (Figure 11B, cross-sections J and K) and over the outer portion of the downstream channel (cross-sections M and N). Lower-velocity flow from the Wabash River is confined between the mixing interface and the inner bank of the bend and gradually accelerates in the downstream channel (cross-sections M and N). Similar to patterns observed for M_r <1, the contrast in downstream velocity between the flows weakens here (cross-sections M and N); yet surficial water temperature patterns again indicate a lack of mixing as the temperature differential extends linearly downstream (Figure 12B).

Two counter-rotating, surface-convergent helical cells are apparent within the central region of the confluent meander bend when M_r > 1 (Figure 11B, cross-sections J and K). The clockwise-rotating cell over the outer (west) portion of the confluence presumably forms when high-momentum fluid from the tributary undergoes slight curvature upon entering the junction. Helicity within both cells flanking the mixing interface is strongest at the upstream end of the confluence (cross-sections J and K), but weakens and becomes less organized in the downstream channel, especially within the cell on the tributary (west) side of the interface (cross-sections M and N).

5 Discussion

Analysis of patterns of 3-D fluid motion at the two sites investigated in this study reveal both similarities and significant differences in the response of flow structure between high angle and low angle confluent meander bends to changes in M_r. At both high and low angle confluent meander bends, a zone of flow stagnation characterized by a zone of low-velocity fluid near the upstream junction corner and responds to changes in M_r by this zone extending into the upstream channel of the river with the lowest momentum flux. For $M_r < 1$, high velocity flow extends across most of the curving main channel as it enters the junction, presumably increasing the curvature-induced cross-stream water surface gradient and enhancing the adverse pressure gradient that produces flow stagnation near the upstream junction corner. This effect has been shown to increase stagnation at experimental confluent meander bends (Roberts, 2004). For $M_r < 1$, the zone of stagnation can extend into the tributary channel. At ORWR, an elongated stagnation zone along the outer bank of the Wabash River segregates the high-velocity cores of the confluent rivers by displacing the core of the tributary inward (Figure 9A, cross-section D); whereas at WRVR, the momentum flux of the Vermilion River is so low compared to the main river that flow stagnates across nearly the entire tributary channel as momentum from the high-velocity core of the Wabash River expands rapidly outward in the downstream channel (Figure 11A, cross-sections B, K-N). For $M_r > 1$, flow stagnation is replaced by a broad zone of high-velocity flow across the tributary channel at both sites (Figure 9B, cross-section A; Figure 11B, cross-section B). A region of flow stagnation wraps around the upstream junction corner over the outer portion of the main channel, restricting the high-velocity core of the main river to the center and inner portions of the meander bend immediately upstream of the confluence (Figure 9B, cross-section J; Figure 11B, cross-sections F and I).

The mutual deflection of converging flows in the central region of each confluence generates a well-developed mixing interface defined at the surface by abrupt changes in surficial water temperature, the magnitude of depth-averaged velocity vectors, and patterns of secondary flow. Both the location and angle at which the tributary enters the curving main river largely control the extent of flow deflection. At the high-angle junction of ORWR, the Wabash River joins the Ohio River at the apex of a bend in the main channel such that the flow fields of the rivers are nearly orthogonal to one another as they converge. The abrupt turning of flow from the Wabash River to align with the orientation of the downstream channel is similar to patterns of deflection-induced curvature of the lateral tributary at asymmetrical confluences (Best, 1987; Rhoads and Sukhodolov, 2001). Turning of tributary flow is enhanced when $M_r < 1$ as a result of the outward shift of the mixing interface that confines flow from the tributary to a narrow path between the interface and outer bank of the bend (Figure 9A, cross-sections L and N). Increased penetration of tributary flow into the confluence when $M_r > 1$ deflects flow from the main river inward (Figure 13), although the presence of an inflowing tributary at the bend apex deflects main river flow away from the outer bank even for $M_r < 0.5$ (Riley and Rhoads, 2012) and is comparable to deflection of main river flow away from the mouth of the lateral tributary at asymmetrical junctions (Best, 1987; Rhoads and Sukhodolov, 2001).

Flow deflection is less pronounced at WRVR, where the small angle of tributary entry downstream of a bend apex on the Wabash River results in converging flows that nearly parallel one another. Consequently, the position of the mixing interface at the upstream end of the confluence where the flows initially meet remains generally unchanged between measurement dates (Figures 11 A,B, cross-section J). Because penetration of tributary flow into the confluence is greatly reduced compared to ORWR, the Vermilion River is ineffective at deflecting flow from the Wabash River away from the outer bank of the meander bend in the downstream channel when $M_r < 1$ (Figure 14A). The low frequency of tributary-dominant flows at WRVR with the capability of performing change to the receiving channel (Figure 2D) indicates that momentum from the main river may routinely be transferred outward across most of the downstream channel and deflect tributary flow against the outer bank, much in the same way that flow is deflected toward the bank opposite from the dominant tributary at symmetrical confluences (Mosley, 1976). The geometry imparted by the confluence planform, including low junction angle and nearly linear alignment of the tributary with the downstream channel, prevents tributary flow from penetrating the center of the junction and downstream portion of the bend, even when $M_r > 1$ (Figure 14B). During these infrequent conditions, the high-velocity core of the tributary persists over the outer portion of the downstream channel and restricts flow from the main river to the center and inner portions of the bend.

This study is among the first to document coherent patterns of secondary circulation in confluences of large rivers with beds consisting of coarse sand and fine gravel. Large-scale helical motion at ORWR and WRVR appears to arise from local imbalances between centrifugal and pressure-gradient forces associated with channel curvature of one or both of the confluent rivers immediately upstream of the junction along with curvature of flow within the confluence. Spatial patterns of helicity differ between the high-angle (ORWR) and low-angle (WRVR) confluent meander bends due largely to the extent of upstream flow curvature and degree of turning of tributary flow into the downstream channel. Flow structure inherited from curvature of both the main and tributary channels upstream of ORWR yields two distinct counter-rotating, surface-convergent helical cells within the confluence (Figures 9A,B, cross-sections L and N). Opposing patterns of flow curvature within the central region of the junction, which have been shown to induce helicity at asymmetrical and symmetrical confluences with concordant beds (Ashmore et al., 1992; Rhoads and Kenworthy, 1995, 1998; Rhoads, 1996; Bradbrook et al., 2000; Rhoads and Sukhodolov, 2001), reinforce patterns of fluid rotation within the dual helical cells and enhance lateral advection of near-surface downstream momentum toward the mixing interface. Both helical cells persist in the downstream channel, although the size of the cells depends strongly on M_r. The cells weaken substantially approximately one channel width downstream from the center of the confluence as the hydraulic impacts of the confluence on flow patterns diminish.

The results indicate that when tributary channels are relatively straight (e.g., WRVR), helical motion does not develop in the tributary upstream of the confluence. In such cases, helical motion inherited from flow curvature on the main river occupies most of the downstream channel when $M_r < 1$ (Figure 14A). Low-velocity tributary flow is unable to deflect high-momentum, near-surface fluid advected laterally by the helical cell away from the outer portion of the channel. Thus the overall pattern of fluid motion at the junction for low M_r is almost entirely dictated by helical motion through the meander bend (Figure 14A). For $M_r > 1$, the high-velocity core of the tributary confines a less organized helical cell from the main river to the center and inner portion of the bend (Figure 14B). A second helical cell with clockwise circulation emerges over the outer portion of the downstream channel as the accelerated tributary flow curves slightly upon entering the confluence. These counter-rotating cells weaken and begin to dissipate in the downstream channel.

Patterns of near-surface water temperature reveal a well-defined mixing interface between the converging flows at each site that extends through the cross sections of the downstream channel, indicating little mixing of the flows occurs within the vicinity of either confluence (Figures 10, 12). The mixing interface at the high-angle confluent meander bend (ORWR) is roughly flanked by dual counter-rotating helical cells on each measurement date (Figure 9), similar to patterns identified at a small confluent meander bend with similar junction angle (Riley and Rhoads, 2012). At the low-angle confluent meander bend (WRVR), the interface aligns closely with the margin of the high velocity core of the dominant tributary and the lower velocity of the adjacent subordinate flow (Figure 11). Lateral advection of downstream momentum penetrates the interface, especially for low M_r, yet the temperature differential persists between the main river and tributary flow downstream of the confluence. This lack of mixing between incoming flows, despite the existence of secondary flow, differs from findings at a small asymmetrical confluence where helical motion appears to distort the mixing interface and enhance mixing (Rhoads and Sukhodolov, 2001).

Flow separation has been shown to develop at the angular downstream junction corner of experimental channels (Best and Reid, 1984; Best, 1987; Roberts, 2004), but often is not found at the more rounded corner of natural confluences where tributary flow may remain attached to the channel bank upon turning into the downstream channel (Roy et al., 1988; Roy and Bergeron, 1990; Ashmore et al., 1992; Rhoads and Sukhodolov, 2001). Previous field work at a high-angle confluent meander bend found that tributary flow accelerated upon entering the confluence over the outer portion of the downstream channel to maintain continuity, thereby preventing flow separation (Riley and Rhoads, 2012). The absence of flow separation at the low-angle WRVR is largely attributable to minimal turning of tributary flow into the confluence. The nearly linear configuration of the Vermilion River with the downstream channel allows high velocity fluid from the tributary to remain attached to the bank when $M_r > 1$ (Figure 11B), whereas advection of downstream momentum from the Wabash River across the channel when $M_r < 1$ confines low velocity flow from the tributary to the bank below the downstream junction corner (Figure 11A). A flow separation zone is present on both measurement dates at the high-angle ORWR, although the zone is broader when $M_r > 1$ (Figure 9B). Fluid in the tributary is topographically steered toward the outer bank of the curving channel upstream of the confluence by a point bar along the inner bank. This lateral deflection of flow by morphologic features has also been shown to affect flow separation at a small symmetrical confluence (Rhoads and Sukhodolov, 2001). Increased flow deflection by the Ohio River when $M_r < 1$ forces tributary flow to turn more abruptly into the downstream channel and narrows the flow separation zone (Figure 9A).

The response of bed morphology to changes in M_r differs between ORWR and WRVR, suggesting that differences in junction angle influence the development and spatial extent of geomorphic features at confluent meander bends. At ORWR, the path of the navigation pool in the Ohio River through the confluence (Figure 3A) generally coincides with the position of its high-velocity core and helical cell for low M_r (Figure 9A). Near-bed fluid is directed inward by this cell, sweeping sediment away from the center of the junction and over the face of the broad inner bank point bar. Extensive rearrangement of bed morphology due to an influx of sediment following a large tributary-dominant discharge event (Zinger et al., 2011) led to the protrusion of a wedge of sediment from the mouth of the Wabash River into the center of the confluence that disrupted the curvilinear path of the pool (Figure 3B). The continued influx of sediment from the tributary and increased penetration of tributary flow for high M_r shifted the pool laterally to a position near the inner bank (Figure 3C). Truncation of the point bar increases channel asymmetry through the center of the confluence and upstream end of the downstream channel. This pattern of bed topography – where the deepest part of the channel is positioned against the inner bank and a bar platform extends over the outer bank – is opposite of the pattern found in most meander bends, but conforms to findings from a small natural confluent meander bend (Riley and Rhoads, 2012).

The comparative uniformity of the channel bed between measurement dates and absence of substantial bed scour at the low-angle WRVR contrasts substantially with the morphodynamics of the high-angle ORWR. While central bed scour is a common feature at many confluences, previous field studies have found that scour can be shallow or even absent from junctions with discordant beds (Biron et al., 1993b) and at confluences with high bed roughness (Roy et al., 1988) and low junction angle. At WRVR, the low angle of tributary entry at the downstream end of a meander bend limits the extent of deflection between the confluent flows, which has been shown to reduce scour depth at the junction of experimental channels (Mosley, 1976; Best, 1988). Furthermore, tributary-dominant flow conditions that may lead to the emergence of a second, counter-rotating helical cell are rare and too short-lived to significantly alter bed morphology (Figures 2B,D). Thus, a small, shallow (< 0.5 m) scour hole is positioned downstream of the junction apex (Figure 5) underlying the upstream end of the mixing interface (Figure 12) on each measurement date.

The relative stability of the bed and minimal scouring at WRVR results in persistence of the Wabash River point bar through the downstream channel. The persistence of the bar at low-angle confluent meander bends is a deviation from the findings of Riley and Rhoads (2012) because tributary flow is ineffective at deflecting flow from the main river inward due to weak flow convergence, but is consistent with patterns of bed morphology typically found in meander bends (Dietrich, 1987). The point bar is constricted by a wide pool near the bend apex, but broadens downstream as channel width increases at the junction (Figure 5). Minor degradation of the bar arises from shifting of the high-velocity core of the Wabash River to the center and inner portion of the channel cross-section due to deflection from high-velocity flow in the Vermilion River when M_r increases.

Two processes have been proposed to explain bar development along the downstream junction corner of confluences – deposition of entrained sediment within a low-velocity zone of separated flow (Best, 1988) and deposition of bedload due to reduced transport capacity (Rhoads and Kenworthy, 1995; Rhoads, 1996; Best and Rhoads, 2008). While Roberts (2004) documented flow separation from the downstream junction corner in laboratory experiments and numerical models of confluent meander bends, the presence of a junction corner bar at a small natural confluent meander bend is likely related to sediment-flux convergence when $M_r > 1$ (Riley and Rhoads, 2012). Bar formation at the junction corner of ORWR is largely due to curvature of the Wabash River immediately upstream of the confluence. The bar forms within a broad region of deposition that begins along the inner bank of the tributary in the upstream channel, where a point bar develops through sediment flux convergence (Nelson and Smith, 1989), and continues around the junction corner into the downstream channel (Figure 3). The bar enlarges below the downstream junction corner for increasing M_r (Figure 4, cross-sections L-O), presumably due to diminished sediment transport capacity along the outer bank as the high-velocity core and helical cell of the tributary penetrate far into the confluence. The bar stores some of the sediment from the meander cutoff and its size is greater than the overlying zone of detached flow (Figure 9), suggesting that deposition of bedload related to patterns of decreasing bed shear stress downstream of the junction corner is primarily responsible for development of the bar, as opposed to flow separation. The absence of flow separation at WRVR and the comparatively linear alignment of the tributary with the downstream channel prevent the development of a junction corner bar.

6 Conclusion

This research contributes to emerging knowledge of the hydro- and morphodynamics of confluent meander bends by investigating the response of 3-D flow structure and bed morphology to changes in M_r at two large confluent meander bends with different tributary entry angles and locations around bends. The results show the importance of junction angle and tributary entry location on flow structure and bed morphology, providing the basis for elaboration of a conceptual model of the dynamics of confluent meander bends based on previous experimental, field, and numerical modeling studies (Roberts, 2004; Riley and Rhoads, 2012). The findings are also consistent with relationships between junction angle and hydrodynamic conditions for asymmetrical and symmetrical confluences (Mosley, 1976; Best, 1987). Strong flow deflection at the high-angle confluent meander bend (ORWR) augments helical motion inherited from flow curvature through meander bends in the main and tributary channels upstream of the junction, producing twin surface-convergent, counter-rotating helical cells that vary in relative size with changes in M_r. This dual cell structure persists through the downstream channel and laterally transfers downstream momentum from the confluent flows toward the mixing interface at the surface. At the low-angle junction (WRVR), the nearly linear configuration of the straight tributary channel with the downstream channel limits the extent of turning of tributary flow at the confluence and inhibits helical motion for prevailing low M_r conditions. Instead, a single large helical cell inherited from flow curvature in the main river upstream of the confluence extends across most of the downstream channel. A weak counter-rotating helical cell forms over the outer portion of the bend for large M_r, when high-velocity fluid from the tributary confines flow from the main river to the center and inner portions of the downstream channel.

The mixing interface at each site is defined by a near-surface water temperature differential between the confluent rivers that extends through the downstream channel. The mixing interface is generally positioned between the helical cells at the high-angle confluence, whereas the interface aligns with the margin of the high-velocity core of the dominant tributary and adjacent low-velocity flow from the subordinate tributary at the low-angle confluence. The persistent temperature differential between flows at both sites suggests that mixing is limited and not greatly enhanced by lateral advection of momentum from helical motion within the confluence and downstream channel – a finding that contrasts with patterns of thermal mixing at smaller confluences with strong helical motion (Rhoads and Kenworthy, 1995; Rhoads and Sukhodolov, 2001). Complete mixing may not occur for a substantial distance downstream of these large river confluences (Mackay, 1970; Stallard, 1987).

Channel and hydrological properties of the tributary largely affect patterns of bed morphology at both sites. A lateral bar at the downstream junction corner of the high-angle confluence is the downstream extension of a larger depositional area that begins with the development of a point bar along the inner bank or the curving tributary channel upstream of the confluence. Tributary flow deflects flow and helical motion in the curving main river away from the outer bank of the bend. A helical cell inherited from curvature of tributary flow upstream of the junction sweeps sediment from the pool over the bar platform, and collectively with flow separation from the downstream junction corner, induces bar development where bank erosion typically occurs downstream of the bend apex (Dietrich, 1987). A broad inner bank point bar on the main river persists through the downstream channel for low M_r, but the inward displacement of the pool by a large influx of sediment into the confluence from the formation of a meander cutoff on the tributary resulted in scour of this bar across from the mouth of the tributary. Enhanced penetration of tributary flow into the confluence for large M_r shifts the mixing interface inward and confines flow and the helical cell of the main river to the inner portion of the bend overlying this region of increased shear stress.

Bed morphology is comparatively stable at the low-angle confluence, where the infrequency and flashiness of tributary-dominant flows prevents substantial adjustment of the bed. The low-angle of tributary entry at the downstream end of a meander bend on the main river limits the extent of flow deflection and produces little bed scour. The inability of tributary flow to penetrate the center and inner portion of the bend, even during large M_r, results in minimal change to the large inner bank point bar on the main river.

Additional studies that document the influence of 1) different configurations between the tributary and main channel, such as the dynamics of a confluent meander bend where the tributary curves in the same direction as the main channel, and 2) different physical and hydrological channel characteristics, including the impact of upstream tributary curvature at confluent meander bends with low junction angles, are needed to more fully ascertain the control each has on confluent meander bend hydro- and morphodynamics. Continued work at the high-angle confluence is of critical importance to document the long-term response of bed morphology at a large confluent meander bend to influxes of sediment from upstream channel change on the tributary and may provide insight into the factors that influence the evolution of this type of confluence planform. The results of this study indicate planform stability may not be related to the development of a bar along the downstream junction corner (Riley and Rhoads, 2012), but rather to the ability of tributary flow to deflect main river flow away from the outer bank and the extent of channel curvature immediately upstream of the junction.

7 Acknowledgments

This research was supported by a grant from the National Science Foundation (BCS-0453316). Thanks to the United States Geological Survey Illinois Water Science Center for use of a boat and data collection equipment, and to Barry Vessels of the Louisville District of the United States Army Corps of Engineers for channel bed data collected in the aftermath of the development of the Wabash River meander cutoff.

8 References

Abrahams AD. 1984a. Channel networks: A geomorphological perspective. *Water Resources Research* **20**(2): 161–168. DOI: 10.1029/WR020i002p00161

Abrahams AD. 1984b. The development of tributaries of different sizes along winding streams and valleys. *Water Resources Research* **20**(12): 1791–1796. DOI: 10.1029/WR020i012p01791

Ashmore P, Parker G. 1983. Confluence scour in coarse braided streams. *Water Resources Research* **19**(2): 392–402. DOI: 10.1029/WR019i002p00392

Ashmore PE, Ferguson RI, Prestegaard KL, Ashworth PJ, Paola C. 1992. Secondary flow in anabranch confluences of a braided, gravel-bed stream. *Earth Surface Processes and Landforms* **17**(3): 299–311. DOI: 10.1002/esp.3290170308

Best JL. 1986. The morphology of river channel confluences. *Progress in Physical Geography* **10**: 157–174. DOI: 10.1177/030913338601000201

Best JL. 1987. Flow dynamics at river channel confluences: Implications for sediment transport and bed morphology. In *Recent Developments in Fluvial Sedimentology: Society of Economic Paleontologists and Mineralogists Special Publication No. 39*, Ethridge FG, Flores RM, Harvey MD (eds). Society for Sedimentary Geology: Tulsa, OK; 27–35. DOI: 10.2110/pec.87.39.0027

Best JL. 1988. Sediment transport and bed morphology at river channel confluences. *Sedimentology* **35**: 481–498. DOI: 10.1111/j.1365-3091.1988.tb00999.x

Best JL, Reid I. 1984. Separation zone at open channel junctions. *Journal of Hydraulic Engineering* **110**(11): 1588–1594. DOI: 10.1061/(ASCE)0733-9429(1984)110:11(1588)

Best JL, Roy AG. 1991. Mixing-layer distortion at the confluence of channels of different depths. *Nature* **350**: 411–413. DOI: 10.1038/350411a0

Best JL, Ashworth PJ. 1997. Scour in large braided rivers and the recognition of sequence stratigraphic boundaries. *Nature* **387**: 275–277. DOI: 10.1038/387275a0

Best JL, Rhoads BL. 2008. Sediment transport, bed morphology and the sedimentology of river channel confluences. In *River Confluences, Tributaries and the Fluvial Network*, Rice SP, Roy AG, Rhoads BL (eds). John Wiley & Sons Ltd.: Chichester, UK; 45–72. DOI: 10.1002/9780470760383.ch4

Biron P, DeSerres B, Roy AG, Best JL. 1993a. Shear layer turbulence at an unequal depth channel confluence. In *Turbulence: Perspectives on Flow and Sediment Transport*, Clifford NJ, French JR, Hardisty J (eds). John Wiley & Sons Ltd.: Chichester, UK; 197–213.

Biron P, Roy AG, Best JL, Boyer CJ. 1993b. Bed morphology and sedimentology at the confluence of unequal depth channels. *Geomorphology* **8**: 115–129. DOI: 10.1016/0169-555x(93)90032-w

Biron P, Best JL, Roy AG. 1996a. Effects of bed discordance on flow dynamics at open channel confluences. *Journal of Hydraulic Engineering* **122**(12): 676–682. DOI: 10.1061/(ASCE)0733-9429(1996)122:12(676)

Biron P, Roy AG, Best JL. 1996b. Turbulent flow structure at concordant and discordant open-channel confluences. *Experiments in Fluids* **21**: 437–446. DOI: 10.1007/BF00189046

Boyer C, Roy AG, Best JL. 2006. Dynamics of a river channel confluence with discordant beds: Flow turbulence, bed load sediment transport, and bed morphology. *Journal of Geophysical Research* **111**: F04007. DOI: 10.1029/2005JF000458

Bradbrook KF, Biron PM, Lane SN, Richards KS, Roy AG. 1998. Investigation of controls on secondary circulation in a simple confluence geometry using a three-dimensional numerical model. *Hydrological Processes* **12**: 1371–1396. DOI: 10.1002/(SICI)1099-1085(19980630)12:8<1371::AID-HYP620>3.0.CO;2-C

Bradbrook KF, Lane SN, Richards KS. 2000. Numerical simulation of three-dimensional time-averaged flow structure at river channel confluences. *Water Resources Research* **36**(9): 2731–2746. DOI: 10.1029/2000WR900011

Bradbrook KF, Lane SN, Richards KS, Biron PM, Roy AG. 2001. Role of bed discordance at asymmetrical river confluences. *Journal of Hydraulic Engineering* **127**(5): 351–368. DOI: 10.1061/(ASCE)0733-9429(2001)127:5(351)

Bridge JS. 1993. The interaction between channel geometry, water flow, sediment transport and deposition in braided rivers. In *Braided Rivers*, Best JL, Bristow CS (eds). Geological Society of London, Special Publication 75; 13–71. DOI: 10.1144/GSL.SP.1993.075.01.02

Bristow CS, Best JL, Roy AG. 1993. Morphology and facies models of channel confluences. In *Alluvial Sedimentation*, Marzo M, Puigdefábregas C (eds). International Association of Sedimentologists, Special Publication 17; 91–100. DOI: 10.1002/9781444303995.ch8

Callaway C. 1902. On a cause of river curves. *The Geological Magazine, New Series, Decade IV* **9**: 450–455.

Constantinescu GS, Miyawaki S, Rhoads B, Sukhodolov A, Kirkil G. 2011. Structure of turbulent flow at a river confluence with momentum and velocity ratios close to 1: Insight provided by an eddy-resolving numerical simulation. *Water Resources Research* **47**: W05507. DOI: 10.1029/2010WR010018

Davis WM. 1903. The development of river meanders. *The Geological Magazine, New Series, Decade IV* **10**: 145–148.

DeSerres B, Roy AG, Biron PM, Best JL. 1999. Three-dimensional structure of flow at a confluence of river channels with discordant beds. *Geomorphology* **26**(4): 313–335. DOI: 10.1016/S0169-555X(98)00064-6

Dietrich WE. 1987. Mechanics of flow and sediment transport in river bends. In *River Channels: Environment and Process*, Richards KS (ed). Basil Blackwell: Oxford, UK; 179–227.

Dinehart RL, Burau JR. 2005a. Averaged indicators of secondary flow in repeated acoustic Doppler current profiler crossings of bends. *Water Resources Research* **41**: W09405. DOI: 10.1029/2005WR004050

Dinehart RL, Burau JR. 2005b. Repeated surveys by acoustic Doppler current profiler for flow and sediment dynamics in a tidal river. *Journal of Hydrology* **314**: 1–21. DOI: 10.1016/j.jhydrol.2005.03.019

Flint J-J. 1980. Tributary arrangements in fluvial systems. *American Journal of Science* **280**: 26–45. DOI: 10.2475/ajs.280.1.26

Hills R. 1983. *Tributary confluences on meandering streams in Minnesota*. Unpublished Survey.

Kenworthy ST, Rhoads BL. 1995. Hydrologic control of spatial patterns of suspended sediment concentration at a stream confluence. *Journal of Hydrology* **168**: 251–263. DOI: 10.1016/0022-1694(94)02644-Q

Lane SN, Bradbrook KF, Richards KS, Biron PM, Roy AG. 2000. Secondary circulation cells in river channel confluences: Measurement artefacts or coherent flow structures? *Hydrological Processes* **14**: 2047–2071. DOI: 10.1002/1099-1085(20000815/30)14:11/12<2047::AID-HYP54>3.0.CO;2-4

Lane SN, Parsons DR, Best JL, Orfeo O, Kostachuk R, Hardy RJ. 2008. Causes of rapid mixing at a junction of two large rivers: Rio Paraná´ and Rio Paraguay, Argentina. *Journal of Geophysical Research* **113**: F02024. DOI: 10.1029/2006JF000745

Mackay JR. 1970. Lateral mixing of the Liard and Mackenzie rivers downstream from their confluence. *Canadian Journal of Earth Sciences* **7**: 111–124. DOI: 10.1139/e70-008

McLelland SJ, Ashworth PJ, Best JL. 1996. The origin and downstream development of coherent flow structures at channel junctions. In *Coherent Flow Structures in Open Channels*, Ashworth PJ, Bennett SJ, Best JL, McLelland SJ (eds). John Wiley & Sons Ltd.: Chichester, UK; 459–490.

McLelland SJ, Ashworth PJ, Best JL, Roden J, Klaassen GJ. 1999. Flow structure and spatial distribution of suspended sediment around an evolving braid bar, Jamuna River, Bangladesh. In *Fluvial Sedimentology VI: Special Publication Number 28 of the International Association of Sedimentologists*, Smith ND, Rogers J (eds). Blackwell Science: London, UK; 43–57.

Mosley MP. 1976. An experimental study of channel confluences. *Journal of Geology* **84**: 535–562. DOI: 10.1086/628230

Muste M, Yu K, Spasojevic M. 2004. Practical aspects of ADCP data use for quantification of mean river flow characteristics; Part I: Moving-vessel measurements. *Flow Measurement and Instrumentation* **15**(1): 1–16. DOI: 10.1016/j.flowmeasinst.2003.09.001

Nelson JM, Smith JD. 1989. Flow in meandering channels with natural topography. In *River Meandering*, Ikeda S, Parker G (eds). Water Resources Monograph, American Geophysical Union: Washington, DC; 69–102. DOI: 10.1029/WM012p0069

Parker G. 1996. Some speculation on the relation between channel morphology and channel-scale flow structures. In *Coherent Flow Structures in Open Channels*, Ashworth PJ, Bennett SJ, Best JL, McLelland SJ (eds). John Wiley & Sons Ltd.: Chichester, UK; 423–458.

Parsons DR, Best JL, Orfeo O, Hardy RJ, Kostaschuk R, Lane SN. 2005. Morphology and flow fields of three-dimensional dunes, Rio Paraná, Argentina: Results from simultaneous multibeam echo sounding and acoustic Doppler current profiling. *Journal of Geophysical Research* **110**: F04S03. DOI: 10.1029/2004JF000231

Parsons DR, Best JL, Lane SN, Orfeo O, Hardy RJ, Kostaschuk R. 2007. Form roughness and the absence of secondary flow in a large confluence-diffluence, Rio Paraná, Argentina. *Earth Surface Processes and Landforms* **32**: 155–162. DOI: 10.1002/esp.1457

Parsons DR, Best JL, Lane SN, Kostaschuk RA, Hardy RJ, Orfeo O, Amsler ML, Szupiany RN. 2008. Large river channel confluences. In *River Confluences, Tributaries, and the Fluvial Network*, Rice SP, Roy AG, Rhoads BL (eds). John Wiley & Sons Ltd.: Chichester, UK; 73–91. DOI: 10.1002/9780470760383.ch5

Parsons DR, Jackson PR, Czuba JA, Engel FL, Rhoads BL, Oberg KA, Best JL, Mueller DS, Johnson KK, Riley JD. 2013. Velocity Mapping Toolbox (VMT): a processing and visualization suite for moving-vessel ADCP measurements. *Earth Surface Processes and Landforms*. DOI: 10.1002/esp.3367

Rhoads BL. 1996. Mean structure of transport-effective flows at an asymmetrical confluence when the main stream is dominant. In *Coherent Flow Structures in Open Channels*, Ashworth PJ, Bennett SJ, Best JL, McLelland SJ (eds). John Wiley & Sons Ltd.: Chichester, UK; 491–517.

Rhoads BL, Kenworthy ST. 1995. Flow structure at an asymmetrical stream confluence. *Geomorphology* **11**: 273–293. DOI: 10.1016/0169-555X(94)00069-4

Rhoads BL, Kenworthy ST. 1998. Time-averaged flow structure in the central region of a stream confluence. *Earth Surface Processes and Landforms* **23**(2): 171–191. DOI: 10.1002/(SICI)1096-9837(199802)23:2<171::AID-ESP842>3.0.CO;2-T

Rhoads BL, Sukhodolov AN. 2001. Field investigation of three-dimensional flow structure at stream confluences: 1. Thermal mixing and time-averaged velocities. *Water Resources Research* **37**: 2393–2410. DOI: 10.1029/2001WR000316

Rhoads BL, Sukhodolov AN. 2004. Spatial and temporal structure of shear layer turbulence at a stream confluence. *Water Resources Research* **40**: W06304. DOI: 10.1029/2003WR002811

Rhoads BL, Sukhodolov AN. 2008. Lateral momentum flux and the spatial evolution of flow within a confluence mixing interface. *Water Resources Research* **44**: W08440. DOI: 10.1029/2007WR006634

Rhoads BL, Riley JD, Mayer DR. 2009. Response of bed morphology and bed material texture to hydrological conditions at an asymmetrical stream confluence. *Geomorphology* **109**: 161–173. DOI: 10.1016/j.geomorph.2009.02.029

Richardson WR, Thorne CR. 1998. Secondary currents around braid bar in Brahmaputra River, Bangladesh. *Journal of Hydraulic Engineering* **124**(3): 325–328. DOI: 10.1061/(ASCE)0733-9429(1998)124:3(325)

Riley JD, Rhoads BL. 2012. Flow structure and channel morphology at a natural confluent meander bend. *Geomorphology* **163**: 84–98. DOI: 10.1016/j.geomorph.2011.06.011

Roberts MVT. 2004. *Flow dynamics at open channel confluent-meander bends*. Ph.D. Thesis, University of Leeds, Leeds, UK.

Roy AG, Bergeron N. 1990. Flow and particle paths at a natural river confluence with coarse bed material. *Geomorphology* **3**: 99–112. DOI: 10.1016/0169-555x(90)90039-s

Roy AG, Roy R, Bergeron N. 1988. Hydraulic geometry and changes in flow velocity at a river confluence with coarse bed material. *Earth Surface Processes and Landforms* **13**: 583–598. DOI: 10.1002/esp.3290130704

Rozovskii IL. 1957. Flow of Water in Bends of Open Channels. Academy of Sciences of the Ukrainian SSR, Kiev, U.S.S.R. (translated from Russian by the Israel Program for Scientific Translations, Jerusalem, 1961).

Stallard RF. 1987. Cross-channel mixing and its effect on sedimentation in the Orinoco River. *Water Resources Research* **23**: 1977–1986. DOI: 10.1029/WR023i010p01977

Szupiany RN, Amsler ML, Best JL, Parsons DR. 2007. Comparison of fixed- and moving-vessel flow measurements with an aDp in a large river. *Journal of Hydraulic Engineering* **133**(12): 1299–1309. DOI: 10.1061/(ASCE)0733-9429(2007)133:12(1299)

Szupiany RN, Amsler ML, Parsons DR, Best JL. 2009. Morphology, flow structure, and suspended bed sediment transport at two large braid-bar confluences. *Water Resources Research* **45**: W05415. DOI: 10.1029/2008WR007428

Weber LJ, Schumate ED, Mawer N. 2001. Experiments on flow at a 90° open-channel junction. *Journal of Hydraulic Engineering* **127**(5): 340–350. DOI: 10.1061/(ASCE)0733-9429(2001)127:5(340)

Weerakoon SB, Tamai N. 1989. Three-dimensional calculation of flow in river confluences using boundary-fitted coordinates. *Journal of Hydroscience and Hydraulic Engineering* **7**(1): 51–62.

Weerakoon SB, Kawahara Y, Tamai N. 1991. Three-dimensional flow structure in channel confluences of rectangular section. In *Proceedings XXIV Congress*. International Association for Hydraulic Research: Madrid, Spain; A373–A380.

Zinger JA, Rhoads BL, Best JL. 2011. Extreme sediment pulses generated by bend cutoffs along a large meandering river. *Nature Geoscience* **4**: 675–678. DOI: 10.1038/ngeo1260

Table 1. Hydraulic conditions of measured flows at ORWR and WRVR

	May 15, 2008			January 6, 2009			January 9, 2007			February 6, 2008		
	OR	WR	WR/ OR	OR	WR	WR/ OR	WR	VR	VR/ WR	WR	VR	VR/ WR
Q	4,882	2,193	0.45	2,333	2,100	0.90	801	93	0.12	546	559	1.02
V	0.94	0.68	0.72	0.62	0.90	1.45	1.17	0.32	0.27	0.69	1.71	2.47
M	4,589,080	1,491,240	0.32	1,446,460	1,890,000	1.31	933,791	29,689	0.03	378,815	955,670	2.52

Q = discharge (m^3 s^{-1}), V = mean cross-sectional velocity (m s^{-1}), M = momentum flux (kg m s^{-2})

Figure captions

Figure 1. Location map of (A) field sites, (B) USGS and USACE river gages, and measurement cross sections at (C) ORWR and (D) WRVR confluences.

Figure 2. Estimated normalized flood dominance ratios during the field campaign for (A) ORWR and (B) WRVR and duration curves of ratios for a period of 36 years for (C) ORWR and 68.5 years for (D) WRVR, derived from mean daily discharge data at upstream USGS river gages (Ohio River at Cannelton, IN and Wabash River at Mount Carmel, IL for ORWR; Wabash River at Covington, IN and Vermilion River near Danville, IL for WRVR). Dashed lines in A and B and tick marks on duration curves in C and D denote survey dates.

Figure 3. Bed topography at ORWR on (A) May 15, 2008; (B) June 23, 2008; (C) January 6, 2009. Bed elevation data for June 23, 2008 was obtained from USACE.

Figure 4. Channel cross-section profiles at ORWR. Looking upstream; outer (east) bank is right, inner (west) bank is left for cross-sections A-C; outer (north) bank is left, inner (south) bank is right for cross-sections L, N, O, and P.

Figure 5. Bed topography at WRVR on (A) January 9, 2007 and (B) February 6, 2008.

Figure 6. Channel cross-section profiles at WRVR. Looking upstream; outer (west) bank is left, inner (east) bank is right; except cross-section B where north bank is right, south bank is left.

Figure 7. Depth-averaged velocity vectors at ORWR on (A) May 15, 2008 and (B) January 6, 2009.

Figure 8. Depth-averaged velocity vectors at WRVR on (A) January 9, 2007 and (B) February 6, 2008.

Figure 9. Downstream velocities with Rozovskii secondary/vertical velocity vectors at ORWR on (A) May 15, 2008 and (B) January 6, 2009. Looking upstream; outer (east) bank is right, inner (west) bank is left for cross-sections A, D, and E; outer (north) bank is left, inner (south) bank is right for cross-sections I, J, L, N, O, and P. Dashed line indicates approximate location of mixing interface determined by measurements of near-surface water temperature.

Figure 10. Deviation from mean water temperature near the surface at ORWR on (A) May 15, 2008 and (B) January 6, 2009. Dashed line indicates approximate location of mixing interface.

Figure 11. Downstream velocities with Rozovskii secondary/vertical velocity vectors at WRVR on (A) January 9, 2007 and (B) February 6, 2008. Looking upstream; outer (west) bank is left, inner (east) bank is right; except cross-section B where north bank is right, south bank is left.

Figure 12. Deviation from mean water temperature near the surface at WRVR on (A) January 9, 2007 and (B) February 6, 2008. Dashed line indicates approximate location of mixing interface.

Figure 13. Conceptual model of flow structure and bed morphology at high-angle confluent meander bends when $M_r > 1$.

Figure 14. Conceptual model of flow structure and bed morphology at low-angle confluent meander bends when (A) $M_r < 1$ and (B) $M_r > 1$.

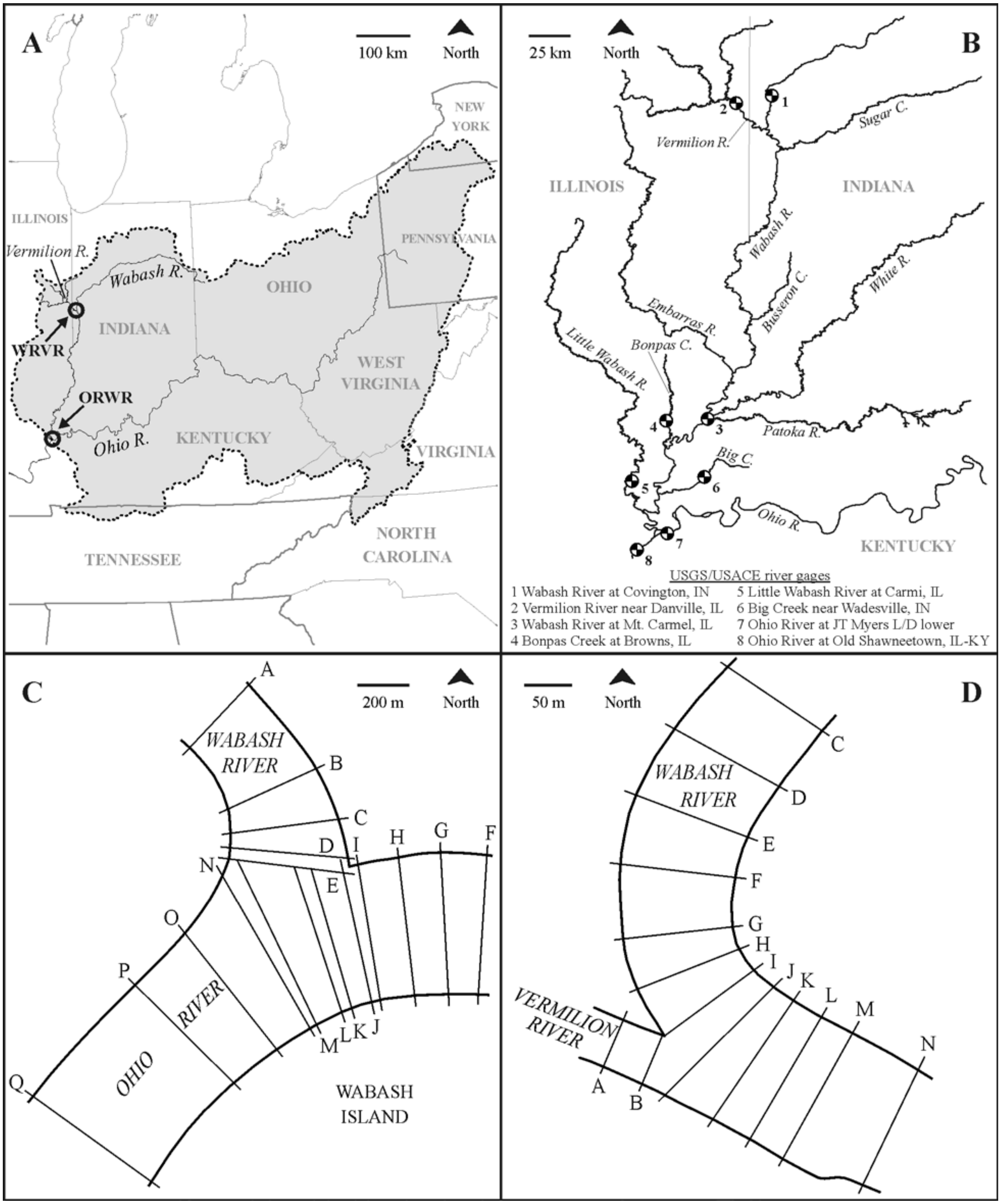
A
100 km
North
NEW YORK
ILLINOIS
Vermilion R.
Wabash R.
OHIO
PENNSYLVANIA
INDIANA
WRVR
WEST VIRGINIA
ORWR
Ohio R.
KENTUCKY
VIRGINIA
NORTH CAROLINA
TENNESSEE
B
25 km
North
Vermilion R.
Sugar C.
ILLINOIS
INDIANA
Wabash R.
White R.
Busseron C.
Embarras R.
Bonpas C.
Little Wabash R.
Patoka R.
Big C.
Ohio R.
KENTUCKY
USGS/USACE river gages
1 Wabash River at Covington, IN
2 Vermilion River near Danville, IL
3 Wabash River at Mt. Carmel, IL
4 Bonpas Creek at Browns, IL
5 Little Wabash River at Carmi, IL
6 Big Creek near Wadesville, IN
7 Ohio River at JT Myers L/D lower
8 Ohio River at Old Shawneetown, IL-KY
C
200 m
North
WABASH RIVER
OHIO RIVER
WABASH ISLAND
D
50 m
North
WABASH RIVER
VERMILION RIVER

Figure 1.

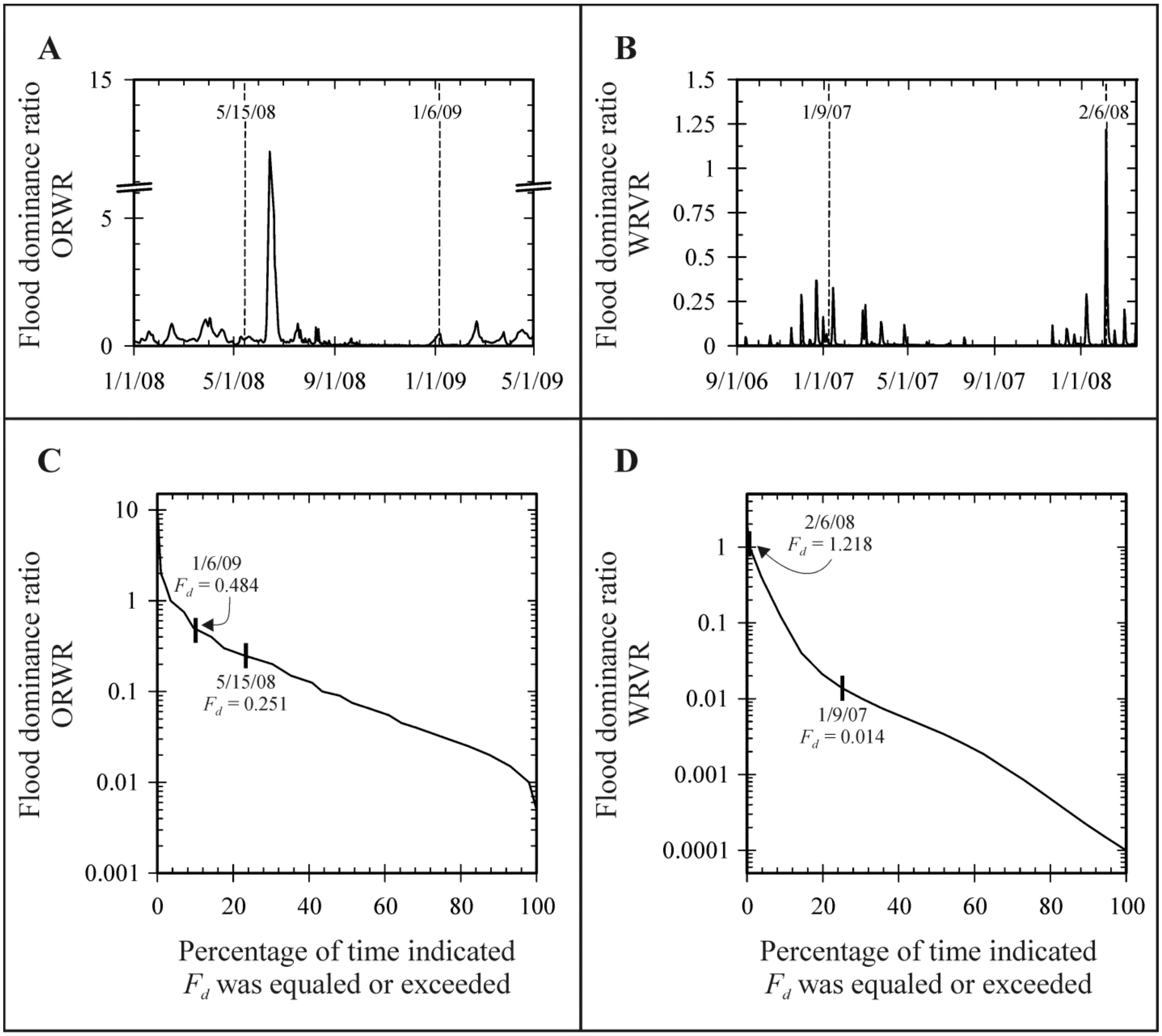
A
Flood dominance ratio
ORWR
15
5
0
5/15/08
1/6/09
1/1/08
5/1/08
9/1/08
1/1/09
5/1/09
B
Flood dominance ratio
WRVR
1.5
1.25
1
0.75
0.5
0.25
0
1/9/07
2/6/08
9/1/06
1/1/07
5/1/07
9/1/07
1/1/08
C
Flood dominance ratio
ORWR
10
1
0.1
0.01
0.001
1/6/09
F_d = 0.484
5/15/08
F_d = 0.251
0
20
40
60
80
100
Percentage of time indicated
F_d was equaled or exceeded
D
Flood dominance ratio
WRVR
1
0.1
0.01
0.001
0.0001
2/6/08
F_d = 1.218
1/9/07
F_d = 0.014
0
20
40
60
80
100
Percentage of time indicated
F_d was equaled or exceeded

Figure 2.

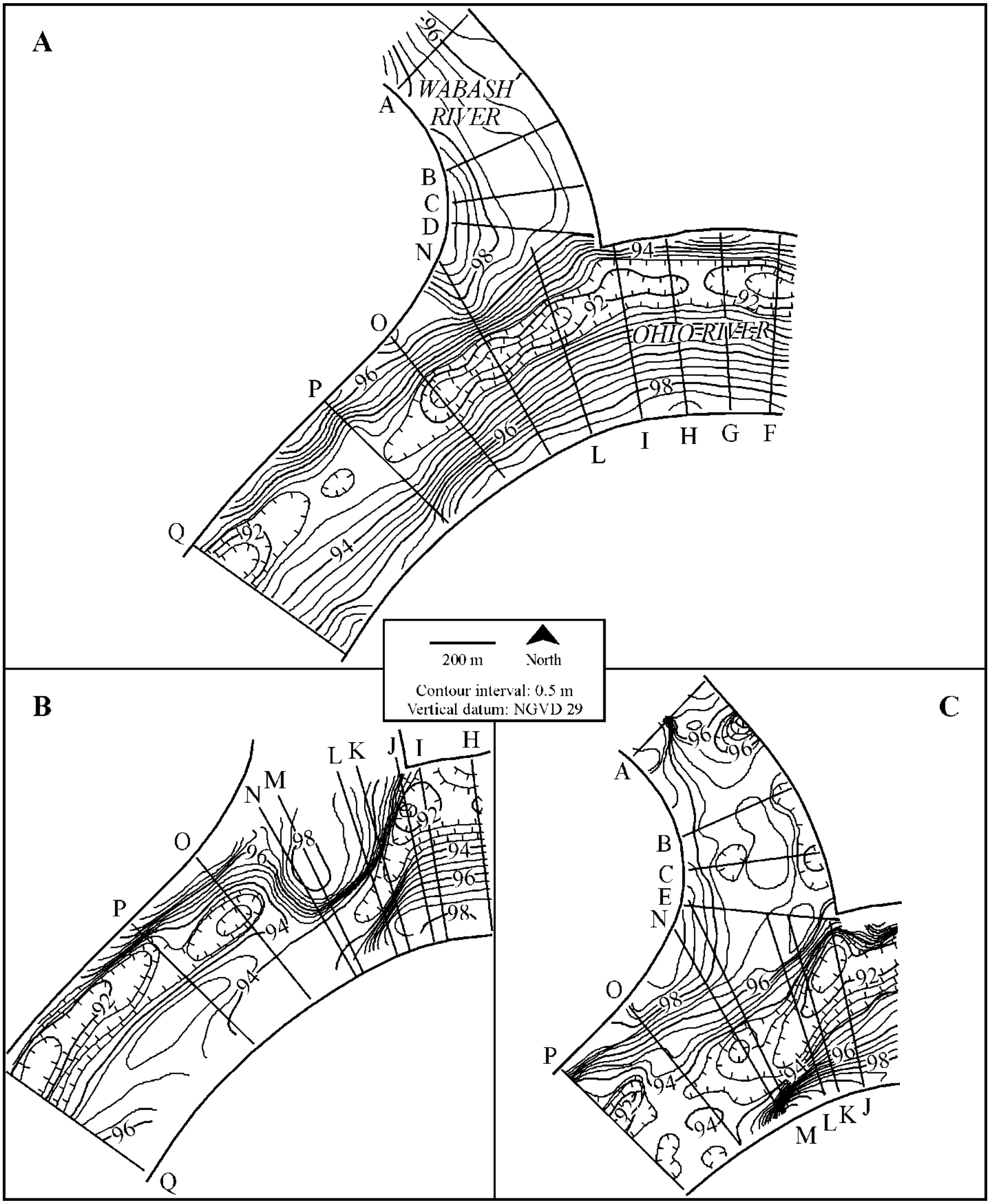
A
WABASH RIVER
OHIO RIVER
B
C
200 m
North
Contour interval: 0.5 m
Vertical datum: NGVD 29

Figure 3.

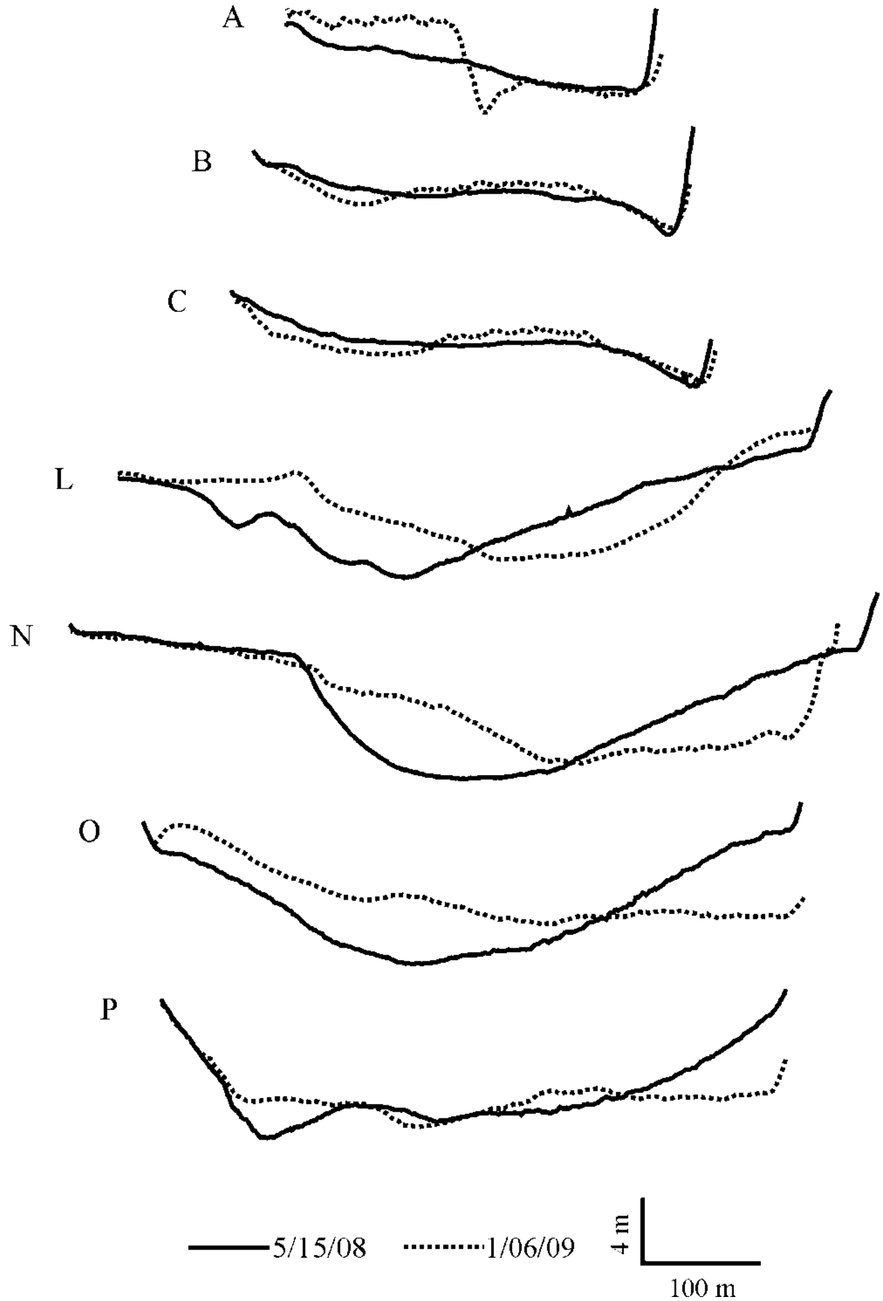

Figure 4.

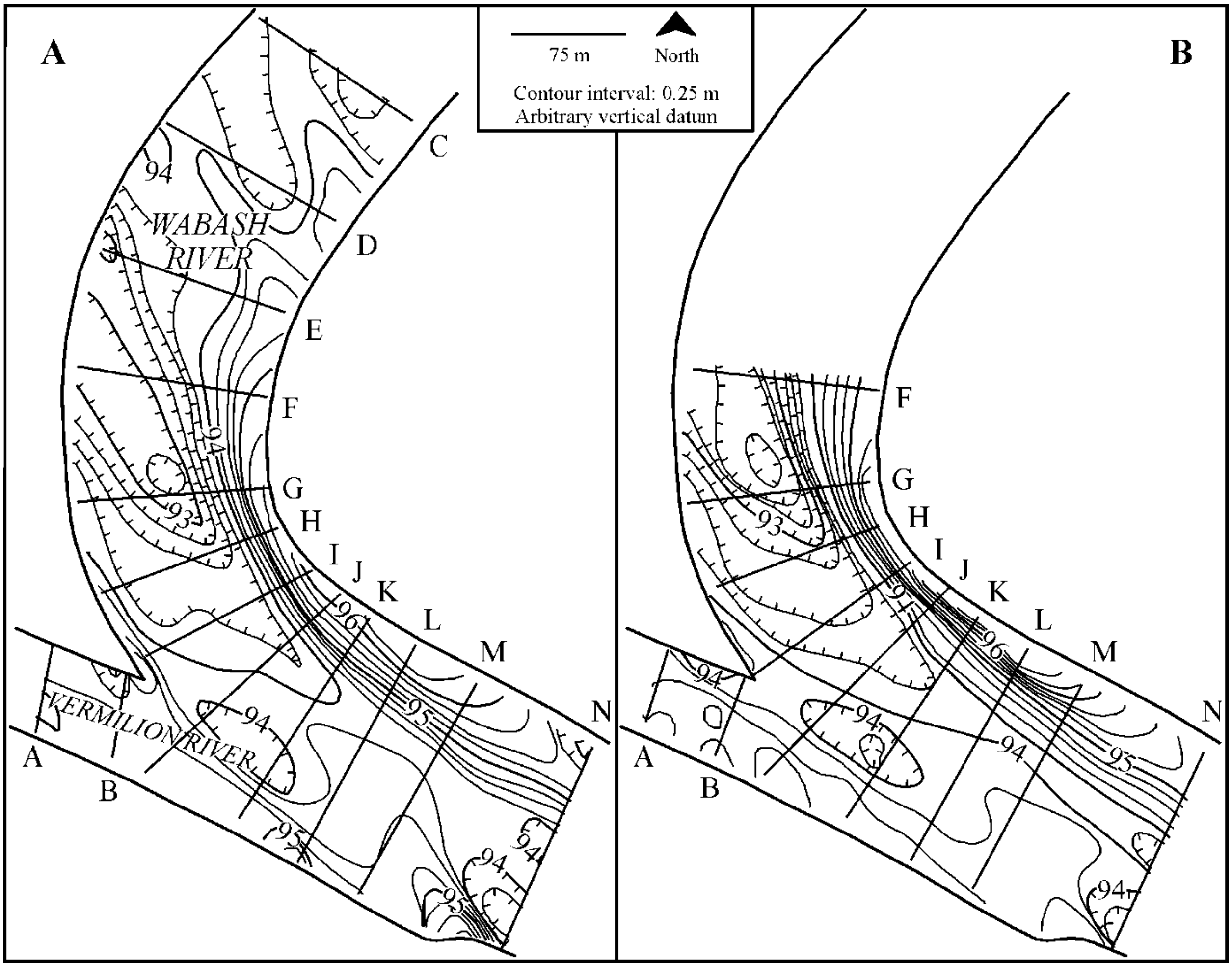
A
B
75 m
North
Contour interval: 0.25 m
Arbitrary vertical datum
WABASH
RIVER
VERMILION RIVER
94
93
95
96
A
B
C
D
E
F
G
H
I
J
K
L
M
N

Figure 5.

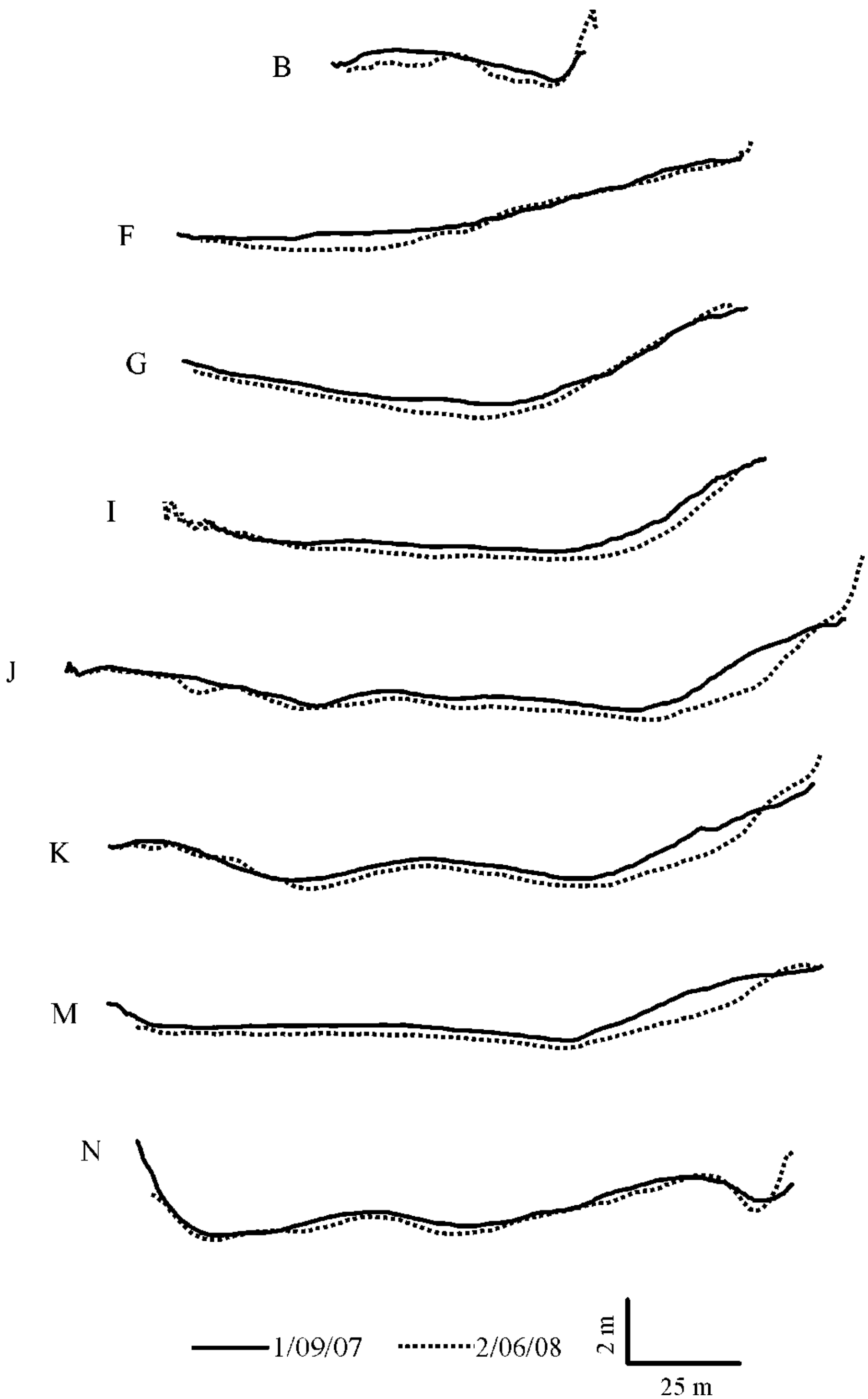

Figure 6.

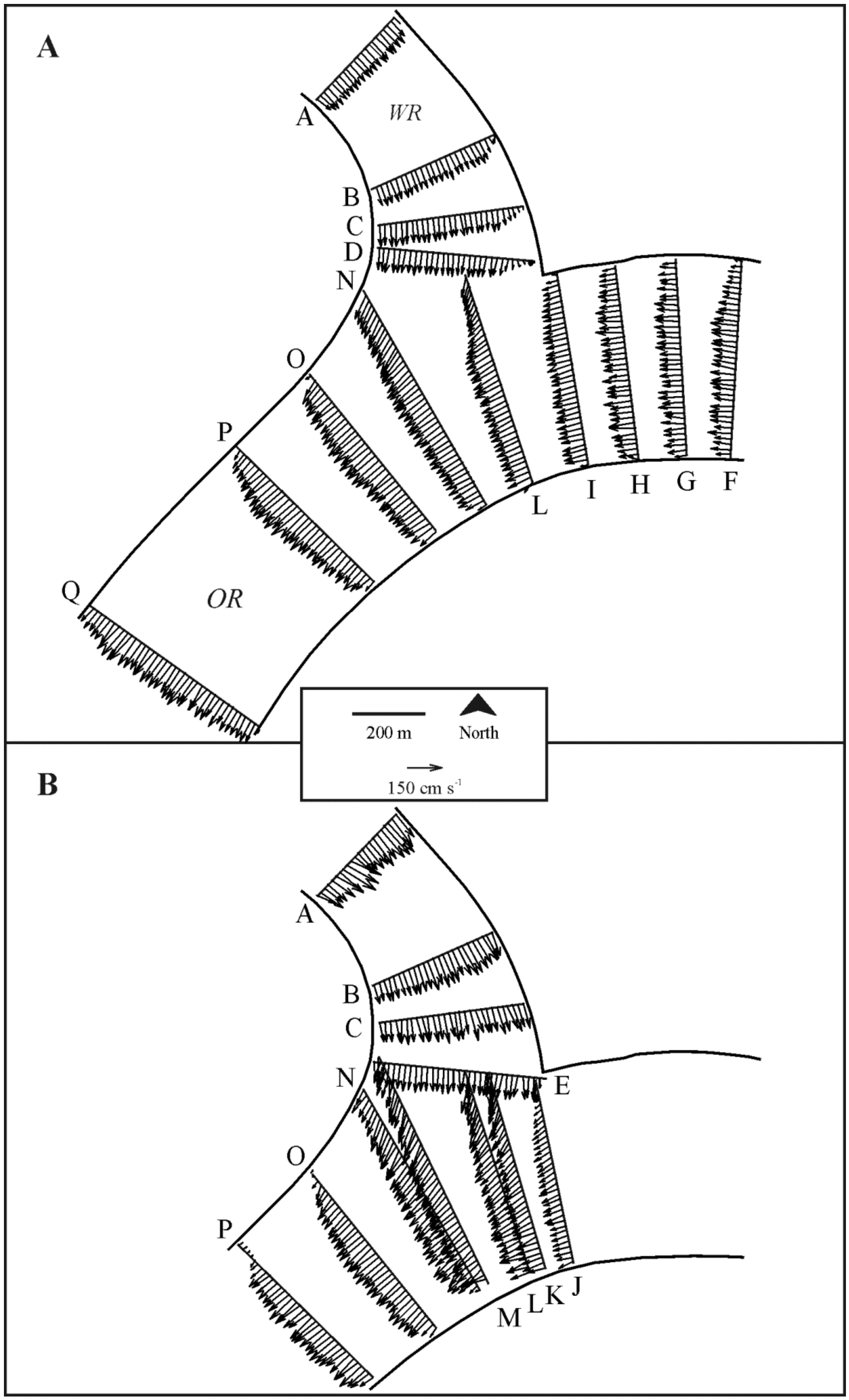

Figure 7.

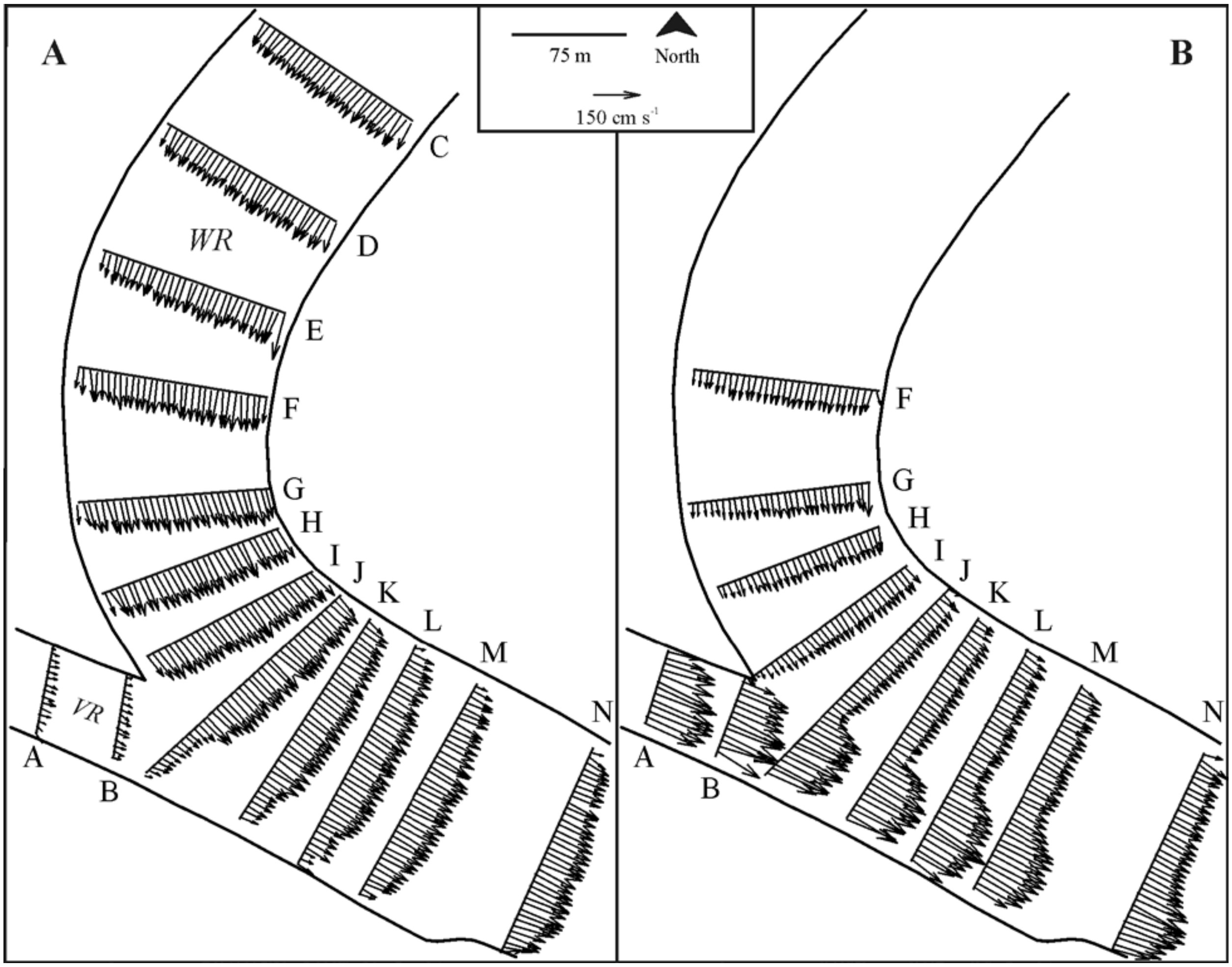

Figure 8.

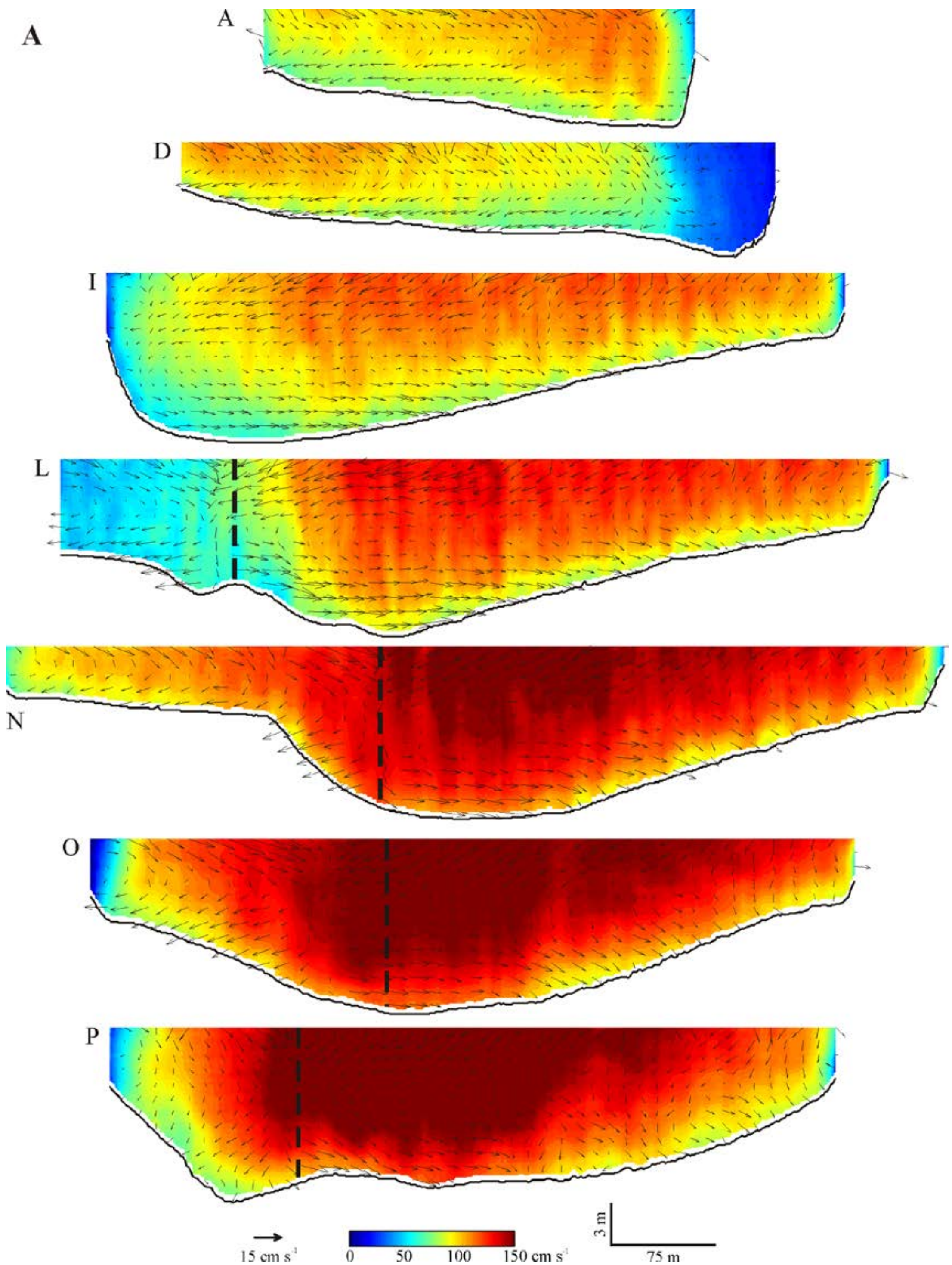

Figure 9.

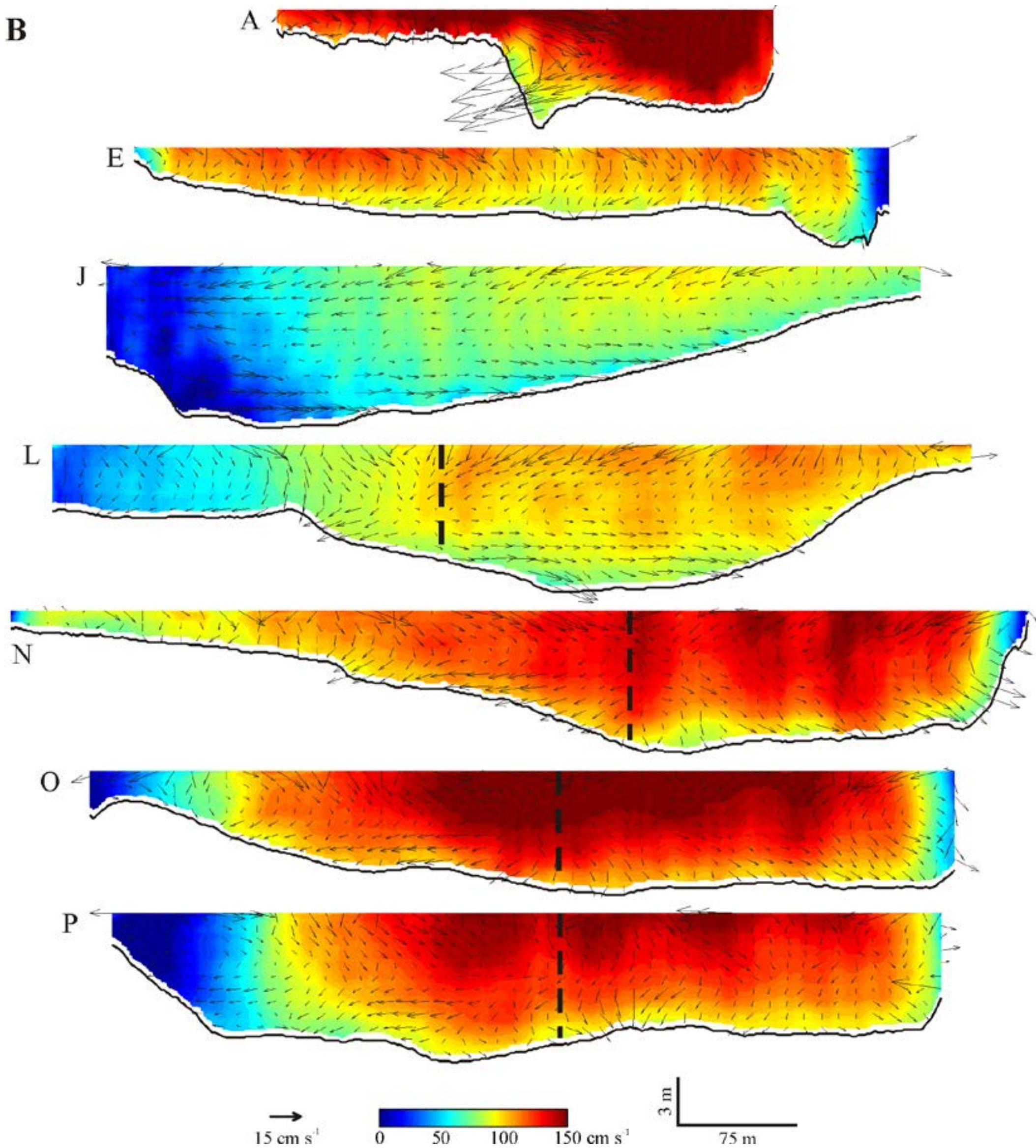

Figure 9. (continued)

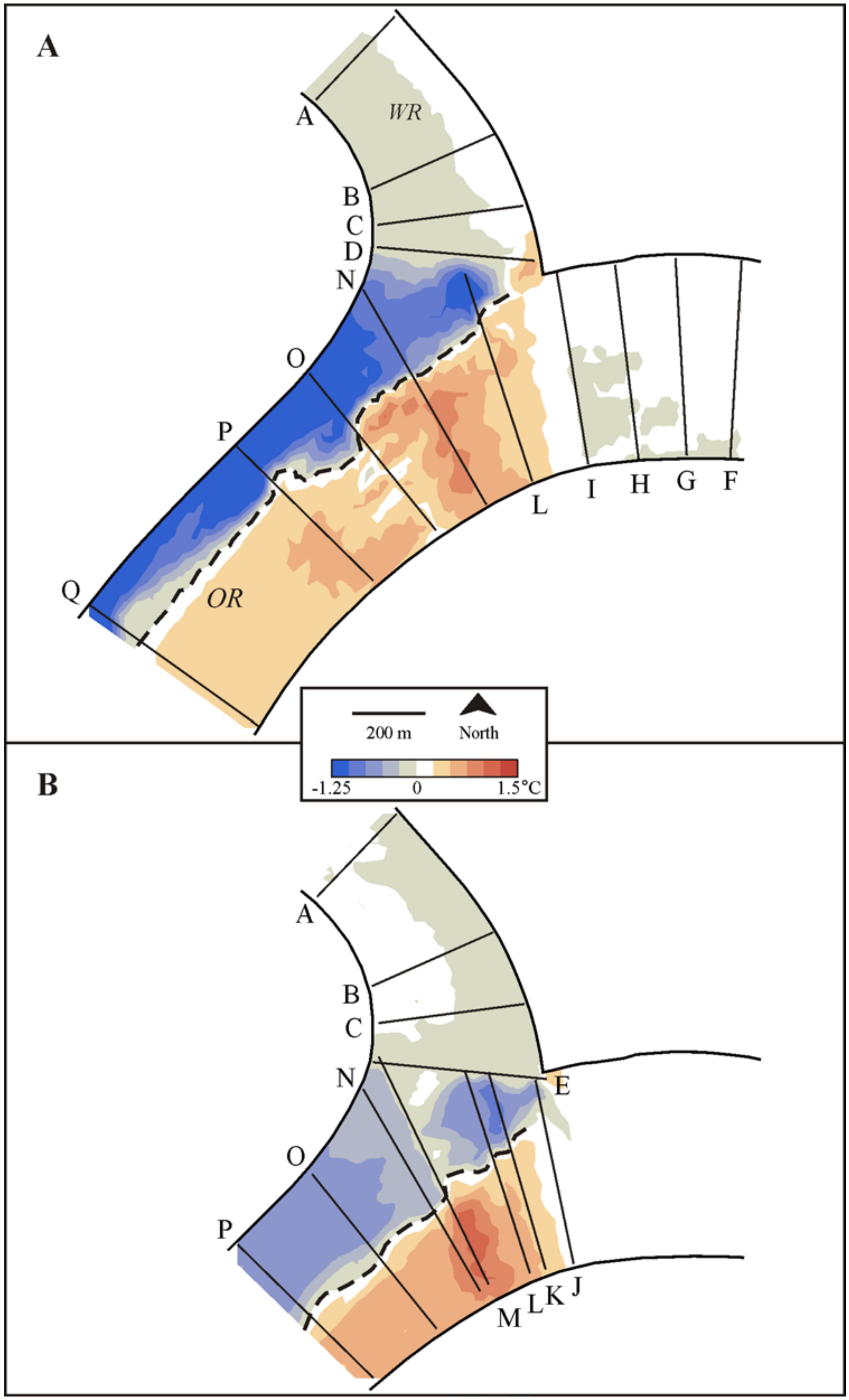

Figure 10.

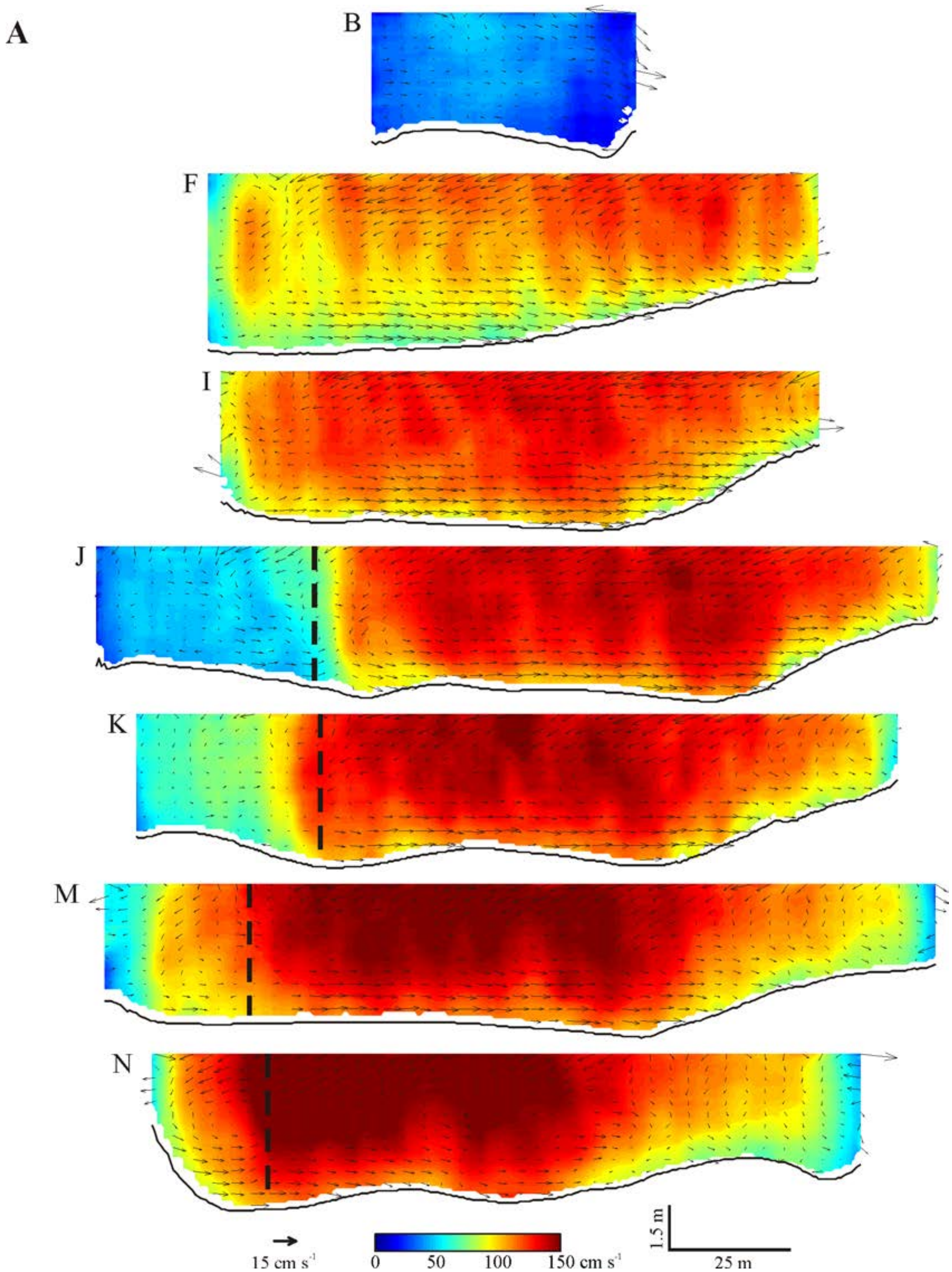

Figure 11.

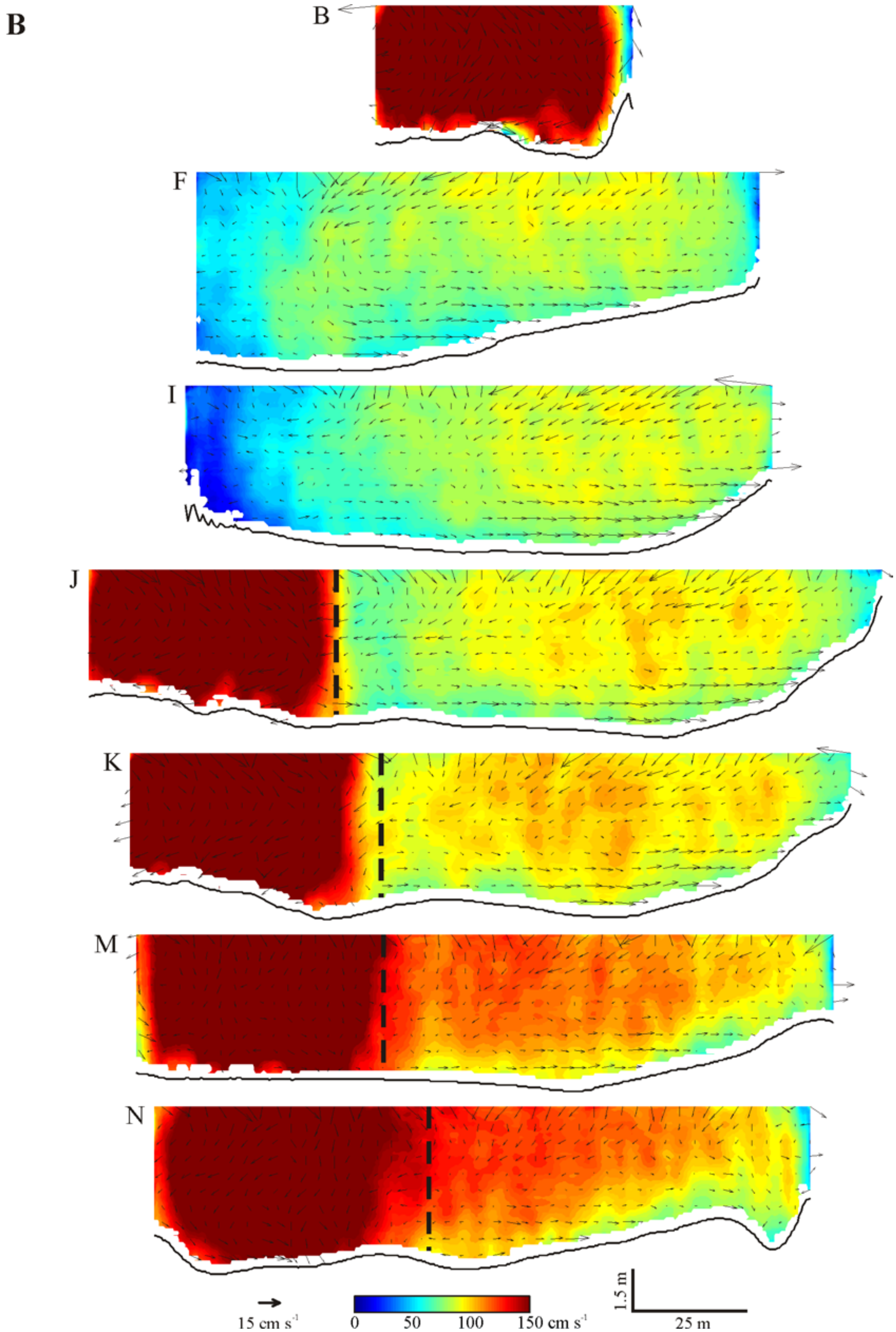

1104

1105 Figure 11. (continued)

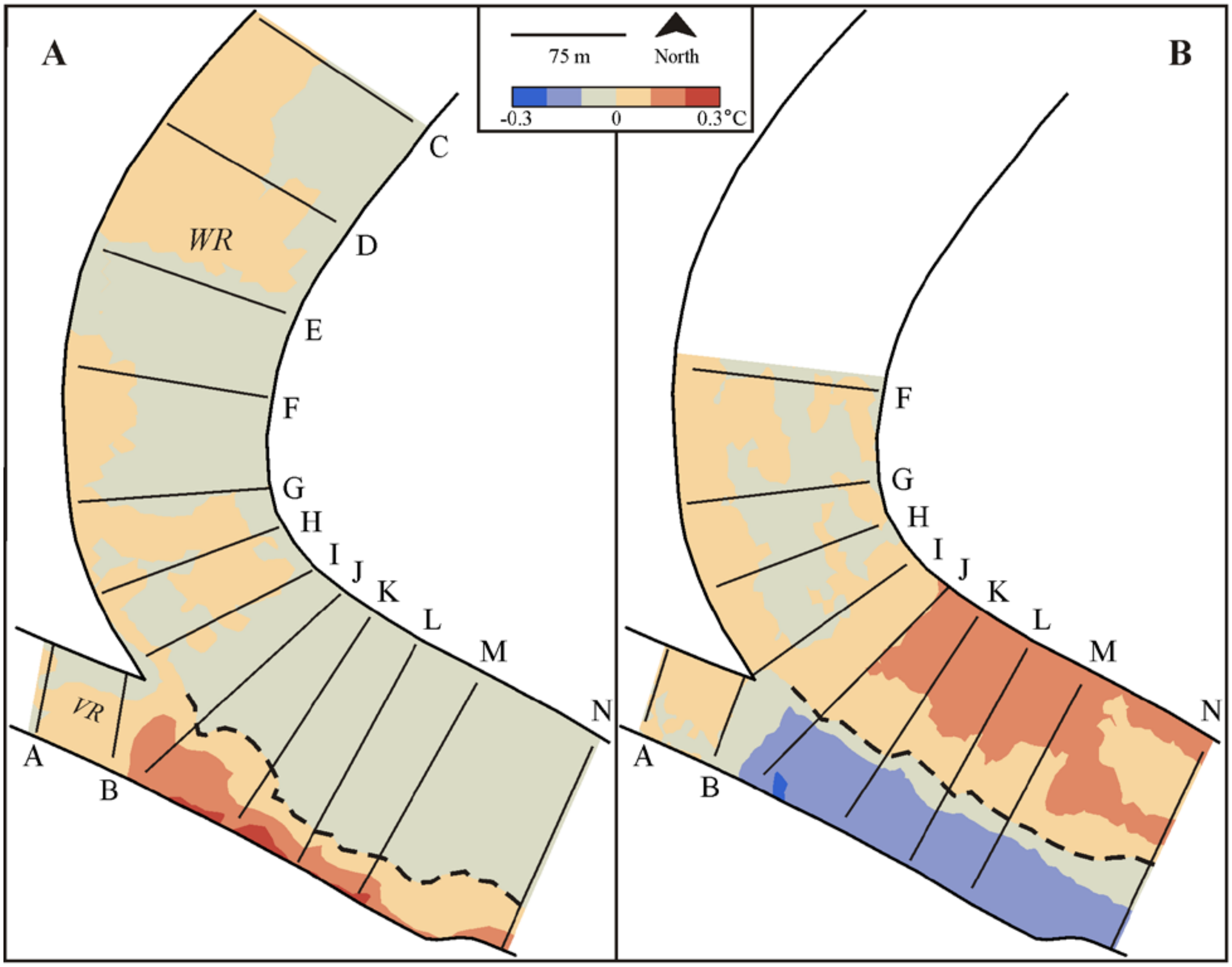

Figure 12.

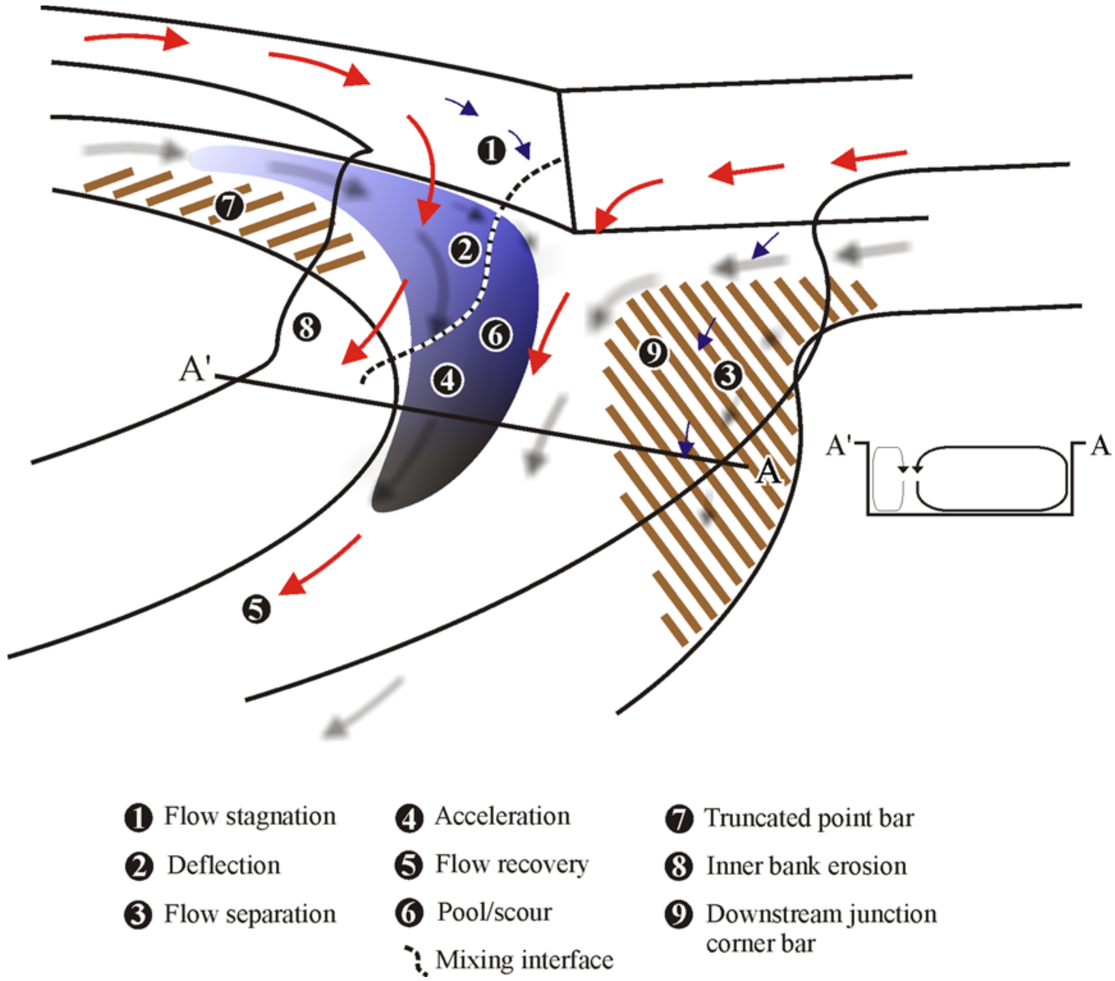
A'
A
A'
A
1 Flow stagnation
2 Deflection
3 Flow separation
4 Acceleration
5 Flow recovery
6 Pool/scour
Mixing interface
7 Truncated point bar
8 Inner bank erosion
9 Downstream junction corner bar

Figure 13.

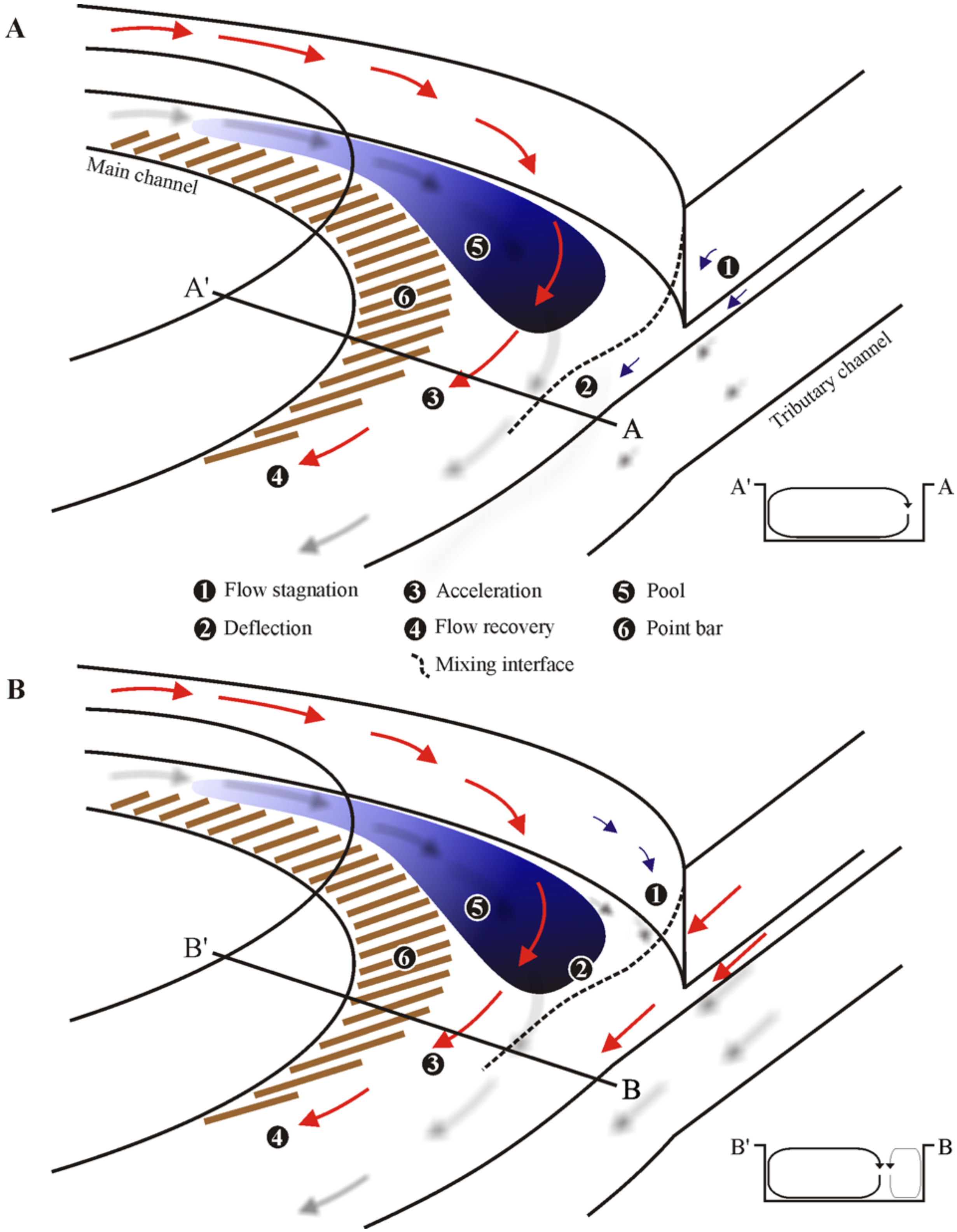
A
Main channel
A'
A
Tributary channel
A'
A
1 Flow stagnation
2 Deflection
3 Acceleration
4 Flow recovery
Mixing interface
5 Pool
6 Point bar
B
B'
B
B'
B

Figure 14.